

We would like to thank the two reviewers for their thorough and constructive reviews of our manuscript. Based on the reviews, we made the following major changes:

- We changed the cited papers referring to methane emissions from sea shelves;
- We split Sect. 4.2 into four sub-parts;
- We acknowledged in Sect. 4.3 the efforts of different teams to measure atmospheric CH₄ in Siberia and Canada and the possibility to further improve our results if these measurements are integrated;
- We revised the caption and the label on the y-axis of Fig. 6. We also showed the significance of difference between the simulations with and without lake emissions using a two-sample *t*-test.

This response file includes: (1) the point-to-point response letter to the first reviewer; (2) the point-to-point response letter to the second reviewer; and (3) a marked-up manuscript version.

1. General Comments

The authors took the time to address the issues pointed at by the first round of reviews. The updated manuscript now successfully presents robust and interesting scientific results. It can now be published with only few remaining technical modifications.

The effort to compare the present results to most of the available literature in Sect. 4.2 is really appreciated, as the works on the Arctic are quite scattered and not often compared in comprehensive reviews.

Response: We appreciate the valuable comments from the reviewer. These comments help us improve the manuscript in both readability and scientific values.

2. Technical comments

p.4 l.83: Shakhova's papers are highly controversial and should not be cited as an absolute reference. More recent works suggest that hydrates emissions to the atmosphere are not that significant in the Arctic. Please prefer some of the following publications rather than Shakhova's. For Svalbard: Grave et al. (2015; doi: 10.1002/2015JC011084), Lund Myhre et al. (2016; doi: 10.1002/2016GL068999). For Laptev: Berchet et al. (2016; doi: 10.5194/acp-16-4147-2016), Stranne et al. (2016; doi: 10.1002/2015GC006119) or Thornton et al. (2016; 15 doi: 10.1002/2016GL068977).

Response: Thank you for indicating this! We added Berchet et al. (2016) and Myhre et al. (2016) as references here and removed Shakhova's paper. In addition, for other places referring to methane emissions from East Siberian Shelf, we also added Thornton et al. (2016) as a reference.

Berchet, A., Bousquet, P., Pison, I., Locatelli, R., Chevallier, F., Paris, J.-D., Dlugokencky, E. J., Laurila, T., Hatakka, J., Viisanen, Y., Worthly, D. E. J., Nisbet, E. G., Fisher, R. E., France, J. L., Lowry, D. and Ivakhov, V.: Atmospheric constraints on the methane emissions from the East Siberian Shelf, *Atmos. Chem. Phys.*, 16, 4147–4157, doi:10.5194/acp-16-4147-2016, 2016.

Myhre, C. L., Ferré, B., Platt, S. M., Silyakova, A., Hermansen, O., Allen, G., Pisso, I., Schmidbauer, N., Stohl, A., Pitt, J., Jansson, P., Greinert, J., Percival, C., Fjaeraa, A. M., O'Shea, S., Gallagher, M., Le Breton, M., Bower, K., Bauguitte, S., Dalsøren, S., Vadakkepuliambatta, S., Fisher, R. E., Nisbet, E. G., Lowry, D., Myhre, G., Pyle, J., Cain, M. and Mienert, J.: Extensive release of methane from Arctic seabed west of Svalbard during summer 2014 does not influence the atmosphere, *Geophys. Res. Lett.*, 43, 4624–4631, doi:10.1002/2016GL068999, 2016.

Thornton, B. F., Geibel, M. C., Crill, P. M., Humborg, C. and Mörrth, C.-M.: Methane fluxes from the sea to the atmosphere across the Siberian shelf seas, *Geophys. Res. Lett.*, 43, 5869–5877, doi:10.1002/2016GL068977, 2016.

p.18 l.388: Sect. 4.1, 4.2, 4.3 are 20, 100 and 30 lines long respectively, which makes the result discussion quite unbalanced. Sect. 4.2 is well structured with high quality content, but please consider splitting it into sub-parts to guide the reader in the discussion.

Response: In the revision, we split Sect. 4.2 into four sub-parts: 4.2.1) Regional CH₄ Emissions; 4.2.2) CH₄ Emissions from Pan-Arctic Lakes; 4.2.3) CH₄ Emissions from Pan-Arctic Wetlands; 4.4.4) Evaluation of Pan-Arctic CH₄ Inversions.

p.11 l.221: in "GEOS-5 meteorological (met)", "met" looks a little bit clumsy when reading it the first time. Maybe replace by something like "GEOS-5 meteorological (hereafter GEOS-5 met)", or more elegant.

Response: We have revised it as suggested.

p.21 l.465: Berchet et al. (2015) applies a regional atmospheric inversion as in this manuscript with surface atmospheric sites and not "flux towers". Please reformulate this sentence.

Response: We have revised this sentence as "Using the atmospheric CH₄ observation data at several sites near Siberian wetlands, Berchet et al. (2015) estimated that CH₄ emissions from Siberian wetlands were in the range of 1–13 Tg CH₄ yr⁻¹, wider than our estimated range."

fig. 1: Siberia looks quite empty here, which is less and less true, fortunately. Somewhere in the discussion should be mentioned the effort by different teams to put instruments in Siberia: JR-STATION by NIES, ZOTTO by MPI, one site near Laptev Sea by FMI, etc. Environment Canada maintains continuous sites in North American Arctic as well. One or two sentences should acknowledge that using all these sites in an inversion system (possible follow-up of the present paper) should improve the inversion results and might reduce (or not?) the gains of using satellite data (though they would be always welcome).

Response: We added the following sentences in our revision: "As shown in Fig. 1, our inverse modeling assimilated few high-precision surface CH₄ measurements in Siberia and northern Canada. Since some efforts have already been made by different teams to measure atmospheric CH₄ routinely in Siberia (e.g., the JR-STATION network by NIES, the Zotino Tall Tower Observatory by MPI-BGC and the Tiksi site by the Finnish Meteorological Institute) and in North American Arctic (e.g., the Behchoko site by Environment Canada), we would like to take advantage of these measurements to further improve our inversion results and re-evaluate the gains of using satellite data in our future studies."

The manuscript has improved significantly, and can be accepted with one final correction: The text describing figure 6 mentions an 'impressive improvement' between the blue and red distributions that are shown. To me, however, they look about the same. The caption doesn't explain the red and blue line extending to the top of the figure, but I guess they represent the means (or medians?). I'm sure that a student t-test of the significance of the difference between these distributions wouldn't justify calling this an 'impressive improvement'. The figure should be explained better in the caption (please also add a label on the y-axis), and the corresponding text should be made compatible with the statistical significance of this result.

Response: We thank the reviewer's valuable comments for helping improve this manuscript. In the revision, we added the label "Number of SCIAMACHY retrievals" on the y-axis. We also added the following description of the extending red and blue lines "Two extending red and blue lines represent the means of the simulation bias under the "DLEM + Lake" scenario and the "DLEM only" scenario, respectively.". We tested the significance of the difference between two simulations using a two-sample t-test (MATLAB "ttest2" function). It shows that their means are significantly different: $p = 0.0032838 < 0.05$. We revised the text accordingly "A further comparison of model-satellite agreement between the DLEM scenario and this no-lake scenario reveals that the agreement improves when lake emissions are considered (see Fig. 6; $p = 0.0032838$ at the two-sample t -test).".

1 Inverse modeling of pan-Arctic methane emissions at high spatial resolution: What
2 can we learn from assimilating satellite retrievals and using different process-based
3 wetland and lake biogeochemical models?

4 Zeli Tan^{1,2}, Qianlai Zhuang^{1,2,3}, Daven K. Henze⁴, Christian Frankenberg⁵, Ed Dlugokencky⁶,
5 Colm Sweeney⁶, Alexander J. Turner⁷, Motoki Sasakawa⁸, Toshinobu Machida⁸

6 ¹Department of Earth, Atmospheric, and Planetary Sciences, Purdue University, West Lafayette,
7 Indiana, USA

8 ²Purdue Climate Change Research Center, Purdue University, West Lafayette, Indiana, USA

9 ³Department of Agronomy, Purdue University, West Lafayette, Indiana, USA

10 ⁴Department of Mechanical Engineering, University of Colorado, Boulder, Colorado, USA

11 ⁵Jet Propulsion Laboratory/California Institute of Technology, Pasadena, California, USA

12 ⁶Global Monitoring Division, NOAA Earth System Research Laboratory, Boulder, Colorado,
13 USA

14 ⁷School of Engineering and Applied Sciences, Harvard University, Cambridge, Massachusetts,
15 USA

16 ⁸National Institute for Environmental Studies, Tsukuba, Japan

17
18 Correspondence to: Qianlai Zhuang (qzhuang@purdue.edu)

Abstract: Understanding methane emissions from the Arctic, a fast warming carbon reservoir, is important for projecting future changes in the global methane cycle. Here we optimized methane emissions from north of 60°N (pan-Arctic) regions using a nested-grid high-resolution inverse model that assimilates both high-precision surface measurements and column-average SCIAMACHY satellite retrievals of methane mole fraction. For the first time, methane emissions from lakes were integrated into an atmospheric transport and inversion estimate, together with prior wetland emissions estimated with ~~by~~ six ~~different~~ biogeochemical models. In our estimates, in 2005, global methane emissions were in the range of 496.4–511.5 Tg yr⁻¹ and pan-Arctic methane emissions were in the range of 11.9–28.5 Tg yr⁻¹. Methane emissions from pan-Arctic wetlands and lakes were 5.5–14.2 Tg yr⁻¹ and 2.4–14.2 Tg yr⁻¹, respectively. Methane emissions from Siberian wetlands and lakes are ~~could be~~ the largest and also have the largest uncertainty. Our results indicate that the uncertainty introduced by different wetland models could be much larger than the uncertainty of each inversion. We also show that assimilating satellite retrievals can reduce the uncertainty of the nested-grid inversions. The significance of lake emissions cannot be identified across the pan-Arctic by high-resolution inversions but it is possible to identify high lake emissions from ~~in~~ some specific regions. In contrast to global inversions, high-resolution nested-grid inversions perform better in estimating near surface CH₄-methane concentrations.

1. Introduction

Methane (CH_4) is the second most powerful carbon-based greenhouse gas in the atmosphere behind carbon dioxide (CO_2) and also plays a significant role in the cycles of ozone, hydroxyl radicals (OH) and stratospheric water vapor (Myhre et al., 2013; Shindell et al., 2009). The atmospheric burden of CH_4 is now more than factor of 2.5 greater than the pre-industrial value of about 700 ppb (Etheridge et al., 1998), mainly due to anthropogenic emissions. Major sources and sinks of CH_4 have been identified (Denman et al., 2007); however their quantification is still of large uncertainties and the annual and inter-annual variability of atmospheric CH_4 are not well explained. For instance, scientists have not yet agreed on what caused the leveling off of atmospheric CH_4 since the 1980s (Dlugokencky et al., 2003; Bousquet et al., 2006; Aydin et al., 2011; Kai et al., 2011; Levin et al., 2012; Simpson et al., 2012; Kirschke et al., 2013) and the recent rebounding of its growth since 2007 (Rigby et al., 2008; Dlugokencky et al., 2009; Nisbet et al., 2014).

To reduce the quantification uncertainty of CH_4 sources and sinks, much effort has been made using Bayesian inference (Bergamaschi et al., 2007, 2009, 2013; Meirink et al., 2008; Cressot et al., 2014; Houweling et al., 2014; Alexe et al., 2015). In these studies, in-situ and/or satellite observations of CH_4 that are representative of large spatial scales were assimilated into a chemical transport model (CTM) to constrain the initial estimates of CH_4 sources and sinks that are inventoried from field studies, industrial investigations and biogeochemical models (Fung et al., 1991; Zhuang et al., 2004; Walter et al., 2006; Zhu et al., 2013; Tan and Zhuang, 2015a and 2015b). Space-borne observations of atmospheric CH_4 are especially useful in inverse modeling because they can deliver dense and continuous coverage unachievable by surface networks or aircraft campaigns (Bergamaschi et al., 2007). There are two types of nadir satellite CH_4

retrievals: one from solar backscatter in the shortwave infrared (SWIR) and the other from thermal infrared radiation (TIR). Between them, SWIR retrievals were more widely used in atmospheric inversion of CH₄ emissions (Bergamaschi et al., 2007, 2009, 2013; Fraser et al., 2013; Cressot et al., 2014; Houweling et al., 2014; Monteil et al., 2014; Wecht et al., 2014; Alexe et al., 2015; Turner et al., 2015) because they can provide column concentrations with near-uniform vertical sensitivity down to the surface. To date, most of the inversions were operated at coarse spatial resolutions over 300 km. However, partly owing to their coarse resolutions, it is impossible for these inversions to constrain different CH₄ sources that are spatially co-located (Fung et al., 1991; Wecht et al., 2014). To address this issue, regional inverse models at fine spatial resolutions were developed (Miller et al., 2013; Wecht et al., 2014; Thompson et al., 2015). For example, Wecht et al. (2014) and Turner et al. (2015) have used the 1/2° × 2/3° horizontal resolution GEOS-Chem adjoint model to constrain CH₄ emissions over North America.

Estimating CH₄ emissions from the Arctic is important for understanding the global carbon cycle because the fast warming of Arctic permafrost, one of the largest organic carbon reservoirs (Tarnocai et al., 2009), could lead to a rapid rise of CH₄ emissions (Zhuang et al., 2006; Walter et al., 2007; Koven et al., 2011). Natural sources dominate the Arctic CH₄ inventory (Fisher et al., 2011), e.g. wetlands (McGuire et al., 2012), lakes (Walter et al., 2006; Bastviken et al., 2011), sea shelves ([Berchet et al., 2016](#); [Myhre et al., 2016](#)~~[Shakhova et al., 2013](#)~~) and oceans (Kort et al., 2012). As the factors governing natural CH₄ production (methanogenesis) and oxidation (methanotrophy) are notoriously heterogeneous, estimates of Arctic CH₄ emissions are still poorly constrained, even with decades of site-level and modeling studies (Zhuang et al., 2004; Bastviken et al., 2011; Schuur et al., 2015; Tan and Zhuang, 2015a; Tan and Zhuang,

2015b). Previous CH₄ inversions over the Arctic only assimilated surface measurements that were too sparse to constrain fine-scale CH₄ fluxes. Also, possibly important CH₄ sources that were newly identified, e.g. CH₄ emissions from Arctic lakes (Walter et al., 2006 and 2007; Bastviken et al., 2011; Tan and Zhuang, 2015a) and the East Siberian Shelf (~~Shakhova et al., 2013~~; Berchet et al., 2016; Thornton et al., 2016) have not been included in these studies. Given the ill-posed nature of trace-gas inversions, realistic prior fluxes could be important for successful inverse modeling of CH₄ emissions from the Arctic (Kaminski and Heimann, 2001).

To address these issues, we used the adjoint of a 3-D CTM at a high spatial resolution (less than 60 km) to improve the quantification of pan-Arctic CH₄ emissions in 2005. We explored the feasibility of using satellite CH₄ retrievals overpassing the pan-Arctic to further constrain regional CH₄ emissions. For the first time, CH₄ emissions from pan-Arctic lakes were included in high-resolution inverse modeling of CH₄ emissions. As wetland emissions are likely the largest pan-Arctic CH₄ source, we also investigated the sensitivity of our estimates to the use of different wetland emission scenarios. Section 2 describes the observation data of atmospheric CH₄ that were used to infer CH₄ emissions and evaluate posterior estimates. Section 3 details the wetland and lake biogeochemical models that were used in this study (Section 3.1), the pan-Arctic nested-grid CTM (Section 3.2), and the adjoint-based inversion method (Section 3.3). Section 4 presents the posterior CH₄ emissions, their evaluation and further discussion.

2. Observations

2.1. Satellite Retrievals

SWIR CH₄ retrievals are available from SCanning Imaging Absorption spectroMeter for Atmospheric CHartographY (SCAMACHY) for 2003–2012 (Frankenberg et al., 2006, 2008, 2011)

and Greenhouse Gases Observing SATellite (GOSAT) for 2009 to present (Parker et al., 2011). SCIAMACHY, aboard the European Space Agency’s environmental research satellite ENVISAT retrieves column-averaged CH₄ mixing ratios (XCH₄) from the SWIR nadir spectra (channel 6: 1.66–1.67 μm) using the IMAP-DOAS algorithm (Frankenberg et al., 2006, 2008, 2011). The satellite operates in a near polar, sun-synchronous orbit at an altitude of 800 km. At channel 6, the ground pixel size of the retrievals is about 30 km (along-track) × 60 km (across-track). We use version 6.0 proxy CH₄ retrievals from Frankenberg et al. (2011) that provide a weighted column average dry-mole fraction of CH₄ with 10-layer averaging kernels and prior CH₄ profiles. The averaging kernels show near-uniform vertical sensitivity in the troposphere and declining sensitivity above the tropopause (Butz et al., 2010). Some auxiliary data, e.g. the air mass factor A_F ($A_F = 1/\cos\theta + 1/\cos\xi$, where θ is the solar zenith angle and ξ is the viewing angle of the satellite), water column density and dry air column density, are also published with the IMAP-DOAS v6.0 XCH₄ product.

The estimated single-retrieval precision is scene-dependent and averages roughly 1.5% or 25 ppb (Frankenberg et al., 2011). With this order of instrument precision, SCIAMACHY cannot resolve day-to-day variability of emissions but can strongly constrain a multi-year average (Turner et al., 2015). The retrieving algorithm firstly calculates CH₄ total column density Ω_{CH_4} (molecules cm⁻²):

$$\Omega_{\text{CH}_4} = \Omega_{\text{A}} + \mathbf{a}^T (\omega - \omega_{\text{A}}) \quad (1)$$

where ω is the true 10-layer sub-column densities of CH₄ (molecules cm⁻²), ω_{A} is the 10-layer prior CH₄ sub-column density (molecules cm⁻²), Ω_{A} is the corresponding a priori CH₄ total column density, and \mathbf{a} is an averaging kernel vector that defines the sensitivity of the retrieved total column to each sub-column in ω . To account for the impact of aerosol scattering and

instrument effects on the observed light path, Frankenberg et al. (2006) used the CO₂ column density Ω_{CO_2} as a proxy to normalize and convert Ω_{CH_4} to a column mixing ratio XCH₄ (ppb):

$$\text{XCH}_4 = \left(\Omega_{\text{CH}_4} / \Omega_{\text{CO}_2} \right) \text{XCO}_2 \quad (2)$$

where XCO₂ is the column-weighted mixing ratio of CO₂ from NOAA's CarbonTracker CO₂ measurement and modeling system. CO₂ is used as a proxy because it is retrieved in a spectrally neighboring fitting window and, relative to CH₄, its mixing ratio is known with much higher precision.

The quality of SCIAMACHY observations is controlled by a filtering scheme that selects only daytime, over land and with cloud free or partially cloud scenes and good fitting accuracy (http://www.temis.nl/climate/docs/TEMIS_SCIA_CH4_IMAPv60_PSD_v2_6.pdf). Further, a surface elevation filter is applied to filter out observations that are different from the model grids at surface altitude by more than 250 m (Bergamaschi et al., 2009; Alexe et al., 2015). This filtering process ensures that the atmospheric columns seen by SCIAMACHY are well represented by the model columns. To avoid spurious outliers that may have a large impact on the inversion, XCH₄ retrievals of less than 1500 ppb or larger than 2500 ppb are discarded (Alexe et al., 2015). For the pan-Arctic, most of qualified XCH₄ retrievals were recorded in the summer time when local solar zenith angles are higher, surface reflectance is lower and impact of Arctic vortex is smaller. Fig. 1 shows the SCIAMACHY retrievals (n = 37743) of the weighted column-average CH₄ dry mixing ratio for July 2005–September 2005 in the pan-Arctic that have passed all quality control tests.

2.2. Surface Observations

The NOAA/ESRL Carbon Cycle Cooperative Global Air Sampling Network provides high-precision weekly flask measurements of surface atmospheric CH₄ dry-air mole fraction (Dlugokencky et al., 2014) that were calibrated against the WMO X2004 CH₄ standard scale maintained at NOAA (Dlugokencky et al., 2005). Due to the coarse resolution of the GEOS-Chem model, we include only marine and continental background sites and exclude sites that are strongly influenced by sub-grid local sources (Alexe et al., 2015), as listed in Table S1. The flask-air samples in the NOAA/ESRL network that were taken from regular ship cruises in Pacific Ocean serve to evaluate simulated surface mixing ratios of global inversions over the remote ocean and downwind the continental sources (Alexe et al., 2015). Fig. 1 shows the Arctic sites that were used for data assimilation and nested-grid inversion evaluation.

2.3. Aircraft Campaign Observations

To derive the bias of SCIAMACHY CH₄ retrievals overpassing the pan-Arctic and evaluate the modeled CH₄ vertical profiles in the troposphere, we used CH₄ measurements that were collected by three aircraft campaigns: the NOAA/ESRL Carbon Cycle Cooperative Global Air Sampling Network's aircraft program (<http://www.esrl.noaa.gov/gmd/ccgg/aircraft/data.html>; Sweeney et al., 2015), the National Institute for Environmental Studies (NIES) aircraft program (Machida et al., 2001; Sasakawa et al., 2013), and the NASA's Arctic Research of the Composition of the Troposphere from Aircraft and Satellite (ARCTAS) mission. For the NOAA/ESRL aircraft mission, CH₄ was routinely collected using 0.7 L silicate glass flasks on planned flights with maximum altitude limits of 300–350 hPa. The sampling vertical resolution is up to 400 m in the boundary layer and all samples were analyzed by NOAA/ESRL in Boulder, Colorado. For the NIES aircraft mission, air samples were collected in 550 mL glass flasks over Surgut, West Siberia (61.5°N, 73.0°E) at altitude ranging from 0.5 to 7 km with 0.5–1.5 km

intervals. The precision of gas chromatograph analysis for CH₄ measurement was estimated to be 1.7 ppb and the NIES-94 scale used in analysis was higher than the NOAA/GMD scale by 3.5–4.6 ppb in a range of 1750–1840 ppb. In ARCTAS, CH₄ was measured over northern Canada by the DACOM tunable diode laser instrument with an estimated accuracy/precision of 1%/0.1%. Central locations of their flights in the pan-Arctic are shown in Fig. 1. Table S2 lists the locations and profiles of the NOAA/ESRL aircraft mission flights used in evaluation.

3. Modeling

Here we describe the prior emissions, the forward model, and the inversion method used to optimize CH₄ emissions in the pan-Arctic on the basis of SCIAMACHY and NOAA/ESRL observations.

3.1. Wetland and Lake CH₄ Emissions

CH₄ emissions estimated by the inverse modeling method can be sensitive to the choice of prior wetland CH₄ fluxes (Bergamaschi, 2007). To assess this sensitivity, we used wetland CH₄ emissions simulated by six well-known wetland biogeochemical models (CLM4Me, DLEM, LPJ-Bern, LPJ-WSL, ORCHIDEE and SDGVM) to setup six different inverse modeling experiments. All wetland CH₄ simulations follow the same protocol of WETland and Wetland CH₄ Inter-comparison of Models Project (WETCHIMP) as described in Melton et al. (2013) and Wania et al. (2013). Melton et al. (2013) demonstrated that the difference of these estimates primarily arises from the model distinction in CH₄ biogeochemistry and wetland hydrology. These models estimated that the annual global CH₄ emissions from wetlands during 2004–2005 were in the range of 121.7–278.1 Tg yr⁻¹ (Fig. S1) and wetland CH₄ emissions are the highest in tropical regions (e.g., Amazon, Southeast Asia and Tropical Africa) where extensive floodplains

and warm environment coexist. In the pan-Arctic, the modeled annual wetland CH₄ emissions in 2005 were in the range of 9.1–20.9 Tg yr⁻¹ (Fig. 2), and their spatial distribution was mainly controlled by the modeled or mapped wetland coverage (Melton et al., 2013). As shown in Fig. 2, because of some consistency in simulating wetland hydrology, nearly all models suggest that there are high CH₄ fluxes in West Siberia Lowlands, Finland and Canadian Shield.

Lakes, permanent still-water bodies without direct connection to the sea, are abundant in the pan-Arctic (Lehner and Döll, 2004). Recent studies indicated that pan-Arctic lakes could contribute a significant amount of CH₄ to the atmosphere (Walter et al., 2006; Tan and Zhuang, 2015a) and the emissions could be driven by factors different from wetland emissions, e.g. the supply of labile yedoma permafrost carbon (Walter et al., 2006) and water deep mixing (Schubert et al., 2012). Because the WETCHIMP models cannot account for this source, we used a one-dimension process-based lake biogeochemical model, bLake4Me, to simulate CH₄ emissions from pan-Arctic lakes (Tan et al., 2015; Tan and Zhuang, 2015a). The bLake4Me model explicitly parameterizes the control of temperature and carbon substrate availability on methanogenesis, the control of temperature and oxygen level on methanotrophy and the transport of gaseous CH₄ by diffusion and ebullition. A detailed model description and evaluation can be found in Tan et al. (2015). Model quantification of CH₄ emissions from all lakes north of 60°N was described by Tan and Zhuang (2015a and 2015b). On average, the estimated CH₄ emissions from pan-Arctic lakes during the studied period are approximately 11 Tg CH₄ yr⁻¹, see Fig. 2.

3.2. GEOS-Chem Model

Atmospheric CH₄ mole fractions are simulated by GEOS-Chem v9-01-03 (<http://acmg.seas.harvard.edu/geos/index.html>), a global 3-D CTM model (Bey et al., 2001). For

the period of 2004–2005, GEOS-Chem is driven by GEOS-5 meteorological ([hereafter GEOS-5](#) met) data from NASA’s Global Modeling Assimilation Office (GMAO). The GEOS-5 met data have horizontal resolution of $1/2^\circ$ latitude \times $2/3^\circ$ longitude, temporal resolution of 6 hours and 72 hybrid sigma-pressure levels extending from Earth’s surface to 0.01 hPa. In contrast to the global GEOS-Chem model, the nested-grid version does not include algorithms for handling advection near the North and South Poles (Lin and Rood, 1996). To avoid polar grid boxes, we crop the native $1/2^\circ \times 2/3^\circ$ resolution GEOS-5 met data to a window region (180°W – 180°E and 80°N – 56°N) for the pan-Arctic nested grid. To make it consistent with the bLake4Me model, only CH_4 emissions north of 60°N are analyzed. We expect that the avoidance of the North Pole only has a minor impact on our inversions because according to Miyazaki et al. (2008) the Northern Hemisphere (NH) extratropics during summer has slow mean-meridional circulation and inactive wave activity but strong vertical transport. Boundary conditions for nested grid simulations are produced using the same period GEOS-Chem $4^\circ \times 5^\circ$ resolution global scale forward runs at 3-hour intervals.

The GEOS-Chem CH_4 simulation was originally introduced by Wang et al. (2004) and updated by Pickett-Heaps et al. (2011). As described by Wecht et al. (2014), the prior anthropogenic sources, including oil/gas production, coal mining, livestock, waste treatment, rice paddies, biofuel burning and other processes, were extracted from Emission Database for Global Atmospheric Research v4.2 (EDGAR4.2) with $0.1^\circ \times 0.1^\circ$ resolution and no seasonality (European Commission, Joint Research Centre/Netherlands Environmental Assessment Agency, 2009). CH_4 emissions from termites and biomass burning were obtained from the study of Fung et al. (1991) and daily Global Fire Emissions Database Version 3 (GFED3) of van der Werf et al. (2010), respectively. CH_4 emissions from wetlands and lakes were simulated by biogeochemical

models described in Section 3.1. Atmospheric CH₄ is mainly removed by tropospheric oxidation initiated by reaction with tropospheric OH, which was computed using a 3-D OH climatology of monthly average concentrations from a previous simulation of tropospheric chemistry (Park et al., 2004). The global mean pressure-weighted tropospheric OH concentration is 10.8×10^5 molecules cm⁻³. For minor sinks, CH₄ uptake by upland soils was derived from Fung et al. (1991) and CH₄ oxidation in the stratosphere was calculated from the archived CH₄ loss frequency described by Murray et al. (2012). The resulting atmospheric lifetime of CH₄ is about 8.9 years, consistent with the observational constraint of 9.1 ± 0.9 years (Prather et al., 2012). We re-gridded and cropped the anthropogenic and natural CH₄ emissions in EDGAR4.2, GFED3 and Fung et al. (1991) for our nested pan-Arctic domain using the Harvard-NASA Emissions Component (HEMCO) software (Keller et al., 2014), marked as “other” in Fig. 2. Compared to CH₄ emissions from natural sources, these emissions are relatively small in 2005 (~ 2.1 Tg yr⁻¹).

3.3. Inversion Method

Atmospheric inversion is a procedure for using observations of atmospheric gases as constraints to estimate surface gas fluxes. The inverse problem can be characterized by solution of

$$\mathbf{y} = \mathbf{F}(\mathbf{x}) + \varepsilon \quad (3)$$

By applying Bayesian theorem and assuming Gaussian errors, the inverse problem can be solved by minimizing the cost function, $J(\mathbf{x})$, that measures the model deviations from both prior assumptions and observations (Enting et al., 2002; Kopacz et al., 2009):

$$J(\mathbf{x}) = (\mathbf{F}(\mathbf{x}) - \mathbf{y})^T \mathbf{C}_d^{-1} (\mathbf{F}(\mathbf{x}) - \mathbf{y}) + \gamma (\mathbf{x} - \mathbf{x}_0)^T \mathbf{C}_{x_0}^{-1} (\mathbf{x} - \mathbf{x}_0) \quad (4)$$

where \mathbf{y} is a vector of observations from SCIAMACHY and NOAA/ESRL, \mathbf{F} is a model operator that maps emissions to observations, \mathbf{x} represents CH_4 emissions to be constrained, \mathbf{x}_0 is the a priori estimate of \mathbf{x} , \mathbf{C}_d is the observational error covariance matrix that includes contributions from model error, representation error (sampling mismatch between observations and the model) and measurement error, and \mathbf{C}_{x_0} is the parameter error covariance matrix (containing the uncertainties of the parameters and their correlations). The regularization parameter γ controls the relative constraints applied by the observational and a priori parts of $J(\mathbf{x})$ (Kopacz et al., 2009). In the adjoint method, γ is not fixed at unity but determined by analyzing its influence on the minimum of $J(\mathbf{x})$ (Henze et al., 2007; Kopacz et al., 2009).

Minimization of $J(\mathbf{x})$ yields the following expression for the maximum a posteriori solution for the state vector $\hat{\mathbf{x}}$ and its associated error covariance $\hat{\mathbf{C}}_x$ (Rodgers, 2000):

$$\hat{\mathbf{x}} = \mathbf{x}_0 + \left((\nabla_{\mathbf{x}} \mathbf{F})^T \mathbf{C}_d^{-1} \nabla_{\mathbf{x}} \mathbf{F} + \gamma \mathbf{C}_{x_0}^{-1} \right)^{-1} (\nabla_{\mathbf{x}} \mathbf{F})^T \mathbf{C}_d^{-1} (\mathbf{y} - \mathbf{F}(\mathbf{x}_0)) \quad (5)$$

$$\hat{\mathbf{C}}_x^{-1} = (\nabla_{\mathbf{x}} \mathbf{F})^T \mathbf{C}_d^{-1} \nabla_{\mathbf{x}} \mathbf{F} + \gamma \mathbf{C}_{x_0}^{-1} \quad (6)$$

where $\nabla_{\mathbf{x}} \mathbf{F}$ is the Jacobian matrix of the forward model. $J(\mathbf{x})$ is minimized iteratively through successive forward and backward simulations with the GEOS-Chem model and its adjoint, developed by Henze et al. (2007) and previously applied to CO , CO_2 and CH_4 source inversions (Jiang et al., 2011; Deng et al., 2014; Wecht et al., 2014). The GEOS-Chem adjoint model is a 4DVAR inverse modeling system that allows optimization of a very large number of parameters using at the same time very large sets of observational data, such as satellite data. Rather than optimizing CH_4 emissions directly, it optimizes an exponential scale factor e_x ($e_x = \ln(\mathbf{x}/\mathbf{x}_0)$) at each grid cell to avoid negative emissions. The posterior error covariance $\hat{\mathbf{C}}_x$ could be

approximated by the Davidon-Fletcher-Powell (DFP) or the Limited-memory Broyden-Fletcher-Goldfarb-Shanno (L-BFGS) optimization algorithm (Singh et al., 2011; Deng et al., 2014). But the performances of these deterministic methods are usually not promising, subjecting to the choice of initial Hessian, so-called preconditioning (Bousserez et al., 2015). In contrast, approximating $\hat{\mathbf{C}}_{\mathbf{x}}$ by stochastic methods, i.e. Monte-Carlo sampling and gradient-based randomization, could help avoid the impact of setting initial Hessian (Bousserez et al., 2015). For example, Bousserez et al. (2015) demonstrated that for high-dimensional inverse problems using a Monte Carlo stochastic approach that samples ensemble members by perturbing \mathbf{x}_0 and \mathbf{y} in line with $\mathbf{C}_{\mathbf{x}_0}$ and $\mathbf{C}_{\mathbf{d}}$ respectively, could guarantee a low relative error (10%) in the variance with as few as 50 members. In this study, the posterior uncertainty of nested-grid inversions was estimated using this method.

For prior emissions, their uncertainties were set as 100% in each grid box and spatial correlation was set as an e-folding function with spatial correlation lengths of 500 km at the global $4^\circ \times 5^\circ$ resolution and of 300 km at the nested grid $1/2^\circ \times 2/3^\circ$ resolution (Bergamaschi et al., 2009). Six global coarse-resolution inversions using different wetland emission scenarios and assimilating both surface CH_4 measurements and satellite CH_4 retrievals were performed during the period of 2005/01–2005/12. These inversions provided boundary conditions for the following nested-grid inversions. For $1/2^\circ \times 2/3^\circ$ nested-grid inversions, we ran the adjoint model for 50 times over the period of 2005/07–2005/09 for each of twelve scenarios: six wetland scenarios by two data assimilation scenarios. The two data assimilation scenarios include one scenario assimilating only NOAA/ESRL measurements and another scenario assimilating both NOAA/ESRL measurements and SCIAMACHY retrievals. As described above, the 50-member ensemble run is for the calculation of posterior estimate uncertainty. The steps to construct

optimal initial conditions for global and nested inversions are described in the supplementary materials. As in Wecht et al. (2014), observations in the first week were not assimilated and each optimization was run iteratively at least 40 times until the reduction of its cost function became less than 0.5% with each successive iteration. In the GEOS-Chem adjoint model, optimization changes its course automatically if local minimum reaches.

3.4. Satellite Retrieval Bias Correction

The importance of bias correction for the assimilation of satellite retrievals has been discussed in many earlier studies (Bergamaschi et al., 2007, 2009, 2013; Fraser et al., 2013; Cressot et al., 2014; Houweling et al., 2014; Wecht et al., 2014; Alexe et al., 2015; Turner et al., 2015). Usually, these studies represented satellite retrieval bias as a regression function of one proxy parameter, i.e. latitude, air mass factor or specific humidity. Air mass factor was used as a proxy parameter by some studies due to its correlation to spectroscopic errors and residual aerosol errors (Cressot et al., 2014; Houweling et al., 2014) and specific humidity was used because water vapor is the main cause of SCIAMACHY seasonal bias that lags the variations of solar zenith angle (Houweling et al., 2014). Relative to air mass factor and humidity, latitude can represent the changes in both solar zenith angle and climate variables (Bergamaschi et al., 2007, 2009 and 2013) and thus was used by more studies. Considering that different proxies can account for different errors, the system bias of satellites may be better represented by multiple proxy parameters.

To test this hypothesis, we compared the performance of three traditional one-proxy methods (latitude φ , air mass factor A_F , specific humidity H_S) and two new two-proxy methods (latitude + humidity, air mass factor + humidity), listed in Table 1. These methods were

evaluated using two reference values: the difference between the satellite-retrieved and the GEOS-Chem modeled CH₄ column mixing ratios and the Bayesian Information Criterion (BIC) score. The BIC criterion is widely used for regression model selection and aims to award a model that fit measurements with the least model parameters. In the study, we would select the bias correction method that gives the smallest difference and the lowest BIC score. In our experiments, all bias correction functions were updated monthly. As listed in Table 1, the “latitude only” correction performs the best among the three single-proxy correction methods and is only slightly worse than the “latitude + humidity” correction method. The “air mass factor only” method does not work as well in our experiment. Turner et al. (2015) suggested that it could be attributed to a potential bias in the GEOS-Chem simulation of CH₄ in the polar stratosphere. As the “latitude + humidity” method has the smallest model-data difference and the lowest BIC score, we applied it for satellite bias correction in all global inversions.

For SCIAMACHY retrievals overpassing the pan-Arctic, because the modeled atmospheric CH₄ could be less reliable, we used another bias correction method. According to a comparison between SCIAMACHY and the high-precision Total Carbon Column Observing Network (TCCON) measurements, the system bias of SCIAMACHY retrievals could be closely correlated with specific humidity averaged over the lowest 3 km of the atmosphere (Houweling et al., 2014). And Wecht et al. (2014) has demonstrated that this humidity-proxy method shows promising performance in debiasing SCIAMACHY retrievals overpassing North America. In this study, we sought a similar linear regression relationship between SCIAMACHY bias and specific humidity. First, we detected the SCIAMACHY bias by comparing SCIAMACHY retrievals with CH₄ vertical profiles measured by the NOAA/ESRL aircraft mission over Alaska, USA, the NIES aircraft mission over Siberia, Russia and the NASA/ARCTAS aircraft mission

over Alberta, Canada. Before comparison, these CH₄ vertical profiles had been mapped to the SCIAMACHY retrieval pressure grid using Eq. (1) and (2). Fig. 3 (left) shows that the retrieved system bias (ΔX_{CH_4}) has a negative relationship with air humidity. Because the pan-Arctic is normally dry, SCIAMACHY retrievals could be lower than atmospheric CH₄ column average mixing ratios in most of days.

After bias correction, the error variances of SCIAMACHY retrievals were estimated using the relative residual error (RRE) method described by Heald et al. (2004). Fig. S2 shows the error variances of SCIAMACHY retrievals in the global scale and Fig. 3 (right) shows the error variances in the nested grid. In both global and nested grid inversions, the total error of individual SCIAMACHY retrievals is assumed to be at least 1.5% (Bergamaschi et al., 2007; Frankenberg et al., 2011). The observational error of the NOAA/ESRL CH₄ mixing ratios is estimated as the sum of measurement error (~0.2%) and representation error. Similar to satellite retrievals, the representation error of surface measurements is defined as the standard deviation of surface CH₄ concentration differences between NOAA/ESRL measurements and GEOS-Chem.

4. Results and Discussion

4.1. Optimized Global CH₄ Emissions

As listed in Table 2, when both NOAA/ESRL measurements and SCIAMACHY retrievals were assimilated, the posterior estimates of total emissions in 2005 show good convergence at a narrow range of 496.4–511.5 Tg CH₄ yr⁻¹, albeit our six prior scenarios span in a wide range (471.5–627.8 Tg CH₄ yr⁻¹). Because the total of global emissions is constrained by the atmospheric CH₄ burden and lifetime, this convergence probably suggests that surface

measurements from the NOAA/ESRL network are of sufficient density and accuracy to represent the global CH₄ burden if the CH₄ lifetime is correct. In contrast, the posterior CH₄ emissions differ largely between different wetland emission scenarios in the TransCom3 land regions. For example, in the DLEM inversion, the estimated CH₄ emissions from the Eurasian temperate region are as large as 146.1 Tg CH₄ yr⁻¹. But in the CLM inversion, the total of these emissions is only 84.9 Tg CH₄ yr⁻¹. Also, for CH₄ emissions from the South American tropical region, the estimate is 31.4 Tg CH₄ yr⁻¹ in the DLEM inversion but nearly two times larger (62.3 Tg CH₄ yr⁻¹) in the SDGVM inversion. There are several possible explanations for the large differences between the scenarios: high-precision surface measurements could be not of sufficient density in regional scales, satellite retrievals could be not of sufficient accuracy, and the GEOS-Chem model and its priors could be not of high temporal and spatial resolutions to resolve satellite retrievals. A detailed comparison between our estimates and previous inversion studies at the global scale is presented in the supplementary materials.

4.2. Optimized Pan-Arctic CH₄ Emissions

4.2.1. Regional CH₄ Emissions

When using both surface measurements and satellite retrievals, our estimated CH₄ emissions over the pan-Arctic are in the range of 11.9–28.5 Tg CH₄ yr⁻¹. The simulation is the largest in the ORCHIDEE scenario and the smallest in the SDGVM scenario: 24.9±3.6 Tg CH₄ yr⁻¹ and 16.1±4.2 Tg CH₄ yr⁻¹, respectively. Regionally, posterior CH₄ emissions from Alaska, northern Canada, northern Europe and Siberia are 0.3–3.4 Tg CH₄ yr⁻¹, 1.3–7.9 Tg CH₄ yr⁻¹, 0.8–8.1 Tg CH₄ yr⁻¹ and 4.4–14.9 Tg CH₄ yr⁻¹, respectively. Same as the global inversions, the difference of the nested-grid inversions between different scenarios is much larger than the total uncertainty of priors and observations of each scenario: 16.6 Tg CH₄ yr⁻¹ vs. 5.5 Tg CH₄ yr⁻¹. In

these regions, CH₄ emissions from Siberia are more uncertain (Fig. 5), a possible indication of the lack of high-quality measurements in Siberia for assimilation. Our results also indicate that the assimilation of SCIAMACHY retrievals overpassing the pan-Arctic can reduce the estimate uncertainty. For example, for the BERN scenario, the posterior uncertainty is about 18%, much smaller than the inversion that only assimilates NOAA/ESRL measurements (27%). And for the CLM scenario, the posterior uncertainty increases from 16% to 23% when only surface measurements were assimilated. Our estimates are consistent with other inverse modeling estimates. For example, Kirschke et al. (2013) reviewed a series of top-down estimation of CH₄ emissions and suggested that CH₄ emissions north of 60°N could be in the range of 12–28 Tg CH₄ yr⁻¹, very close to our estimate. This consistency could reflect the robustness of our nested-grid GEOS-Chem adjoint model and the good constraint of the NOAA/ESRL sites over the pan-Arctic on the atmospheric CH₄ field. Our estimates also imply that CH₄ emission from the pan-Arctic could constitute a large fraction of CH₄ emissions in the northern high latitudes (> 50°N). Based on the estimate (50 Tg CH₄ yr⁻¹) of Monteil et al. (2013), we calculated that 29.2–60.8% of CH₄ emissions in the northern high latitudes could be emitted from the pan-Arctic (> 60°N). For all scenarios, the inverse modeling adjusts total CH₄ emissions downward compared to prior emissions. It is possible that CH₄ emissions are overestimated by the biogeochemical models or double counted between the wetland and lake models or both. This adjustment could also be explained by the underestimate of CH₄ absorption by soils in biogeochemical models due to the missing of high-affinity methanotrophy (Oh et al., 2016).

4.2.2. CH₄ Emissions from Pan-Arctic Lakes

In contrast to CH₄ emissions from pan-Arctic wetlands, CH₄ emissions from pan-Arctic lakes at large spatial scales are still largely unknown. Consensus has not been reached yet on

how to apply the knowledge learnt from individual lakes to the pan-Arctic scale, because even lakes in a small area could have much different transport pathways (ebullition vs. diffusion), morphology (deep vs. shallow and large vs. small), eutrophication (eutrophic vs. oligotrophic) and carbon source (thermokarst vs. non-thermokarst and yedoma vs. non-yedoma). Because wetlands and lakes, both inundation landscapes, are usually neighbored, it is difficult to use inverse modeling at coarse spatial scales to detect strong CH₄ emissions that are emitted solely by lakes. To test whether high-resolution inversions can better represent CH₄ emissions from lakes, we conducted a comparison test (“DLEM only”) over the East Siberia Coastal Lowlands (Fig. 1) using the DLEM model and excluding CH₄ emissions from lakes. We chose the East Siberia Lowlands to test our hypothesis as lakes there occupy 56% of the water-inundated landscapes, i.e. lakes, wetlands and rivers (Lehner and Döll, 2004) and a large fraction of lakes in the region are high-flux yedoma lakes (Walter et al., 2006). We chose the DLEM model considering that the simulated wetland CH₄ emissions in this model are weak for the East Siberia Lowlands. This design is also aimed to alleviate the impact of one major shortcoming: because there are not sufficient high-quality observations, we optimized CH₄ emission in each grid cell separately for wetlands and lakes and in this manner a fraction of lake emissions could be attributed incorrectly to wetlands or vice versa. The inversion of the “DLEM only” scenario is shown in Fig. S5. In comparison to Fig. 4c, CH₄ emissions from the East Siberia Coastal Lowlands are low in Fig. S5. A further comparison of model-satellite agreement between the DLEM scenario and this no-lake scenario reveals that the agreement improves [impressively](#) when lake emissions are considered (see Fig. 6; [p = 0.0032838 at the two-sample t-test](#)). It implies that CH₄ emissions from regional lakes could be significant. As illustrated above, however, the spatial neighborhood of wetlands and lakes makes it difficult to conduct similar

experiments in other areas. Thus we are cautious to claim that CH₄ emissions from lakes are ubiquitously strong across the pan-Arctic. Rather, since we used six wetland models that can simulate very different wetland emission distributions at spatial and temporal scales, our estimates of 2.4–14.2 Tg CH₄ yr⁻¹ for lake emissions could be more useful in explaining the range of this source. The lower bound of our estimate is much smaller than the estimate of 7.1–17.3 Tg CH₄ yr⁻¹ by Bastviken et al. (2011) in the use of extensive site-level observations. In contrast, the upper bound of our estimate is within the range. Given the wide span of this estimate, it is difficult to say whether CH₄ emissions from pan-Arctic lakes can be significant across the region.

4.2.3. CH₄ Emissions from Pan-Arctic Wetlands

Arctic tundra is regarded as an important source of CH₄ in the northern high latitudes. By using process-based models and atmospheric CH₄ observations, McGuire et al. (2012) estimated that Arctic tundra was a source of 25 Tg CH₄ yr⁻¹ to the atmosphere during 1990–2006. By using the TM5-4DVAR inverse model and assimilating SCIAMACHY and NOAA/ESRL observations, Alexe et al. (2015) estimated that CH₄ emissions from Arctic wetlands were 18.2 Tg CH₄ yr⁻¹ for 2010–2011. A similar estimate of 16±5 Tg CH₄ yr⁻¹ was also made by Bruhwiler et al. (2014) using the CarbonTracker-CH₄ assimilation system. Our estimate of 5.5–14.2 Tg CH₄ yr⁻¹ overlaps with the estimate of Bruhwiler et al. (2014) but is much lower than the estimates of Alexe et al. (2015) and McGuire et al. (2012). However, McGuire et al. (2012) did not use complex inverse models and Alexe et al. (2015) used the coarse-resolution TM5-4DVAR inverse model. As our global inversions (Table 2) are consistent with the estimate of Alexe et al. (2015), this difference is likely introduced by the use of the nested-grid inverse model. In other words, the nested-grid inverse model reveals some information that could be missed in global coarse-

resolution inversions. For Siberian wetlands, they could emit much more CH₄ (1.6–7.6 Tg yr⁻¹) than any other areas. But the uncertainty of this source is also the largest. Using [the atmospheric CH₄ observation data at several sites](#) ~~several flux towers~~ near to Siberian wetlands, Berchet et al. (2015) estimated that CH₄ emissions from Siberian wetlands were in the range of 1–13 Tg CH₄ yr⁻¹, wider than our estimated range. In addition, our estimate is also much smaller than the estimate of 21.63 ± 5.25 Tg CH₄ yr⁻¹ by Kim et al. (2012) for annual mean CH₄ emissions from Siberian wetlands during 2005–2010. According to our inversions, CH₄ emissions from wetlands in Alaska, northern Canada, northern Europe are 0–1.2 Tg CH₄ yr⁻¹, 0.4–4.8 Tg CH₄ yr⁻¹ and 0.7–3.6 Tg CH₄ yr⁻¹, respectively. For Alaskan wetlands, the total of posterior CH₄ emissions is much lower than the inferred value of 4.1 Tg CH₄ yr⁻¹ for the Alaskan Yukon River basin during 1986–2005 using the modeling of process-based CH₄ biogeochemistry and large-scale hydrology (Lu and Zhuang, 2012) and also much lower than the inferred value of 3 Tg CH₄ yr⁻¹ for the whole Alaska (Zhuang et al., 2007). Our estimate of wetland emissions from northern Europe compasses a European-scale estimate of 3.6 Tg CH₄ yr⁻¹ by Saarnio et al. (2009), agreeing with the investigation that wetlands in Europe are predominantly located north of 60°N.

4.2.4. Evaluation of Pan-Arctic CH₄ Inversions

As shown in Fig. 7, in most of scenarios, the nested grid inversions perform much better than both the forward simulations and the global inversions at NOAA/ESRL pan-Arctic flask sites (Fig. 1). For example, for the ORCHIDEE scenario, the nested grid inversion reduces the model bias by 44 ppb relative to the forward run and by 20 ppb relative to the global inversion, respectively. Also, for the SDGVM scenario, it reduces the model bias by 22 ppb relative to the forward run and by 13 ppb relative to the global inversion, respectively. But for aircraft CH₄ measurements, it is more complex. The nested grid inversions can reduce the model bias in some

scenarios greatly, i.e. the CLM4Me scenario and the SDGVM scenario. But in many cases, they do not perform visibly better than the forward runs and the global inversions. One possible reason is that the aircraft CH₄ RMS has already been low and thus the remaining errors, including the representation error of model diurnal variability, cannot be resolved by our current inversion system. For example, CH₄ emissions from Alaska can be well constrained by three NOAA/ESRL surface sites in Alaska (BRW, CBA and SHM) and the CH₄ mixing ratios at the aircraft PFA site are representative of the interior of Alaska as pointed out in Sweeney et al. (2015). It is also possible that the increase of grid cells in the nested grid inversions introduced more transport and computation errors.

4.3. Further Discussion

Both the global and nested-grid inversions indicate that the inverse modeling is more sensitive to different wetland models than prior emission error and data error. Thus, to gain better understandings of the global and pan-Arctic CH₄ cycles, it is important to develop more realistic biogeochemical models. Especially, from the perspective of inverse modeling, focus should be on improving the spatial and temporal representation of the models rather than emission magnitude.

For the high-resolution inverse modeling, transport and computation errors of the nested-grid CTMs need to be reduced for better performance. These CTMs can also benefit the efforts to assimilate aircraft CH₄ measurements. For the purpose of satellite data bias correction, more coordination between satellite missions and aircraft missions is demanded. The treatment of the SCIAMACHY bias could be an important uncertainty source for our estimates, as suggested by

Houweling et al. (2014). Future top-down studies could benefit from a more reasonable bias correction method, even for low bias satellite products, e.g. GOSAT (Alexe et al., 2015).

The attribution of CH₄ fluxes to spatially overlapped sources, e.g. wetlands and lakes, could be problematic for even high-resolution inversions. Carbon isotope measurements ($\delta^{13}\text{CH}_4$) are widely used to separate biogenic and geologic CH₄ sources (Langenfelds et al., 2002) but are not useful for two biogenic sources with similar carbon isotope ratios (Walter et al., 2008; Fisher et al., 2011). In our study, lake and wetland emissions were simulated separately by different models. This raised the possibility of double counting emissions of the two sources. A possible solution is to simulate them together in one earth system model and use a consistent method to identify wetland and lake pixels.

Our nested grid adjoint model currently does not cover the regions near the North Pole. While it could be rare in the summer time, if air mass transports across the Arctic Ocean, it may not be represented in the model. In the following studies, we will adapt the advection algorithm for the polar region from the global adjoint model to the nested-grid model and validate the adaptation. These refinements shall reduce the uncertainty of our estimates. It is also valuable to discuss the integration of other natural CH₄ sources found in the pan-Arctic, such as CH₄ emission from subsea permafrost of East Siberian shelf (~~Shakhova et al., 2013~~[Berchet et al., 2016; Thornton et al., 2016](#)). [As shown in Fig. 1, our inverse modeling assimilated few high-precision surface CH₄ measurements in Siberia and northern Canada. Since some efforts have already been made by different teams to measure atmospheric CH₄ routinely in Siberia \(e.g., the JR-STATION network by NIES, the Zotino Tall Tower Observatory by MPI-BGC and the Tiksi site by the Finnish Meteorological Institute\) and in North American Arctic \(e.g., the Behchoko site by Environment Canada\), we would like to take advantage of these measurements to further](#)

[improve our inversion results and re-evaluate the gains of using satellite data in our future studies.](#)

5. Conclusion

In this study, we used a high-resolution nested-grid adjoint model in the pan-Arctic domain to constrain CH₄ emissions from pan-Arctic wetlands, lakes and anthropogenic sources. The sensitivity of the method to different prior wetland CH₄ fluxes was tested. When assimilating both NOAA/ESRL measurements and SCIAMACHY retrievals, we estimated that in 2005, the total of global CH₄ emissions was in the range of 496.4–511.5 Tg CH₄ yr⁻¹, with wetlands contributing 130.0–203.3 Tg CH₄ yr⁻¹. Both of these estimates are consistent with some widely accepted expert assessments. The estimated CH₄ emissions in the pan-Arctic were in the range of 11.9–28.5 Tg yr⁻¹, with wetland and lake emissions ranging from 5.5 to 14.2 Tg yr⁻¹ and from 2.4 to 14.2 Tg yr⁻¹, respectively. The largest CH₄ emissions in the pan-Arctic are from Siberian wetlands and lakes. The study demonstrates that the assimilation of satellite retrievals can reduce the uncertainty of the nested grid inversions. Evaluation with independent datasets shows that the nested inversions can better improve the representation of CH₄ mixing ratios in lower boundary layer rather than top boundary layer and free troposphere.

Acknowledgements: [We would like to thank the two anonymous reviewers for their thorough and constructive reviews.](#) ~~We would like to~~ [Many thanks are given to](#) the WETCHIMP investigators for making their simulations of wetland methane emissions available. We appreciate the help from Guang-Dih Lei and Bhagirath M. Trivedi at NASA and Robert Yantosca at Harvard for processing nested grid GOES-5 met data and the help from Christoph A.

Keller at Harvard for processing nested grid emission data by HEMCO. This study is supported through projects funded to Q. Z. by the NASA Land Use and Land Cover Change program (NASA-NNX09AI26G), Department of Energy (DE-FG02-08ER64599), the NSF Division of Information and Intelligent Systems (NSF-1028291), and the NSF Carbon and Water in the Earth Program (NSF-0630319). This research is also in part supported by the Director, Office of Science, Office of Biological and Environmental Research of the US Department of Energy under Contract No. DE-AC02-05CH11231 as part of their Earth System Modeling Program. D. K. H. acknowledges NOAA grant no. NA14OAR4310136. A. J. T. was supported by a Department of Energy (DOE) Computational Science Graduate Fellowship (CSGF). The supercomputing resource is provided by Rosen Center for Advanced Computing at Purdue University.

References

- Alexe, M., Bergamaschi, P., Segers, A., Detmers, R., Butz, A., Hasekamp, O., Guerlet, S., Parker, R., Boesch, H., Frankenberg, C., Scheepmaker, R. A., Dlugokencky, E., Sweeney, C., Wofsy, S. C. and Kort, E. A.: Inverse modeling of CH₄ emissions for 2010–2011 using different satellite retrieval products from GOSAT and SCIAMACHY, *Atmos. Chem. Phys.*, 15, 113–133, doi:10.5194/acp-15-113-2015, 2015.
- Aydin, M., Verhulst, K. R., Saltzman, E. S., Battle, M. O., Montzka, S. A, Blake, D. R., Tang, Q. and Prather, M. J.: Recent decreases in fossil-fuel emissions of ethane and methane derived from firn air, *Nature*, 476(7359), 198–201, 2011.

578 Bastviken, D., Tranvik, L., Downing, J., Crill, P. M. and Enrich-Prast, A.: Freshwater methane
579 emissions offset the continental carbon sink, *Science*, 331, 50–50, 2011.

580 Berchet, A., Pison, I., Chevallier, F., Paris, J.-D., Bousquet, P., Bonne, J.-L., Arshinov, M. Y.,
581 Belan, B. D., Cressot, C., Davydov, D. K., Dlugokencky, E. J., Fofonov, A. V., Galanin, A.,
582 Lavrič, J., Machida, T., Parker, R., Sasakawa, M., Spahni, R., Stocker, B. D. and Winderlich, J.:
583 Natural and anthropogenic methane fluxes in Eurasia: a meso-scale quantification by generalized
584 atmospheric inversion, *Biogeosciences*, 12, 5393–5414, doi:10.5194/bg-12-5393-2015, 2015.

585 Berchet, A., Bousquet, P., Pison, I., Locatelli, R., Chevallier, F., Paris, J.-D., Dlugokencky, E. J.,
586 Laurila, T., Hatakka, J., Viisanen, Y., Worthy, D. E. J., Nisbet, E. G., Fisher, R. E., France, J. L.,
587 Lowry, D. and Ivakhov, V.: Atmospheric constraints on the methane emissions from the East
588 Siberian Shelf, *Atmos. Chem. Phys.*, 16, 4147–4157, doi:10.5194/acp-16-4147-2016, 2016.

589 Bergamaschi, P., Krol, M., Dentener, F., Vermeulen, A., Meinhardt, F., Graul, R., Ramonet, M. ,
590 Peters, W. and Dlugokencky, E. J.: Inverse modelling of national and European CH₄ emissions
591 using the atmospheric zoom model TM5, *Atmos. Chem. Phys.*, 5, 2431–2460, 2005.

592 Bergamaschi, P., Frankenberg, C., Meirink, J. F., Krol, M., Dentener, F., Wagner, T., Platt, U.,
593 Kaplan, J. O., Körner, S., Heimann, M., Dlugokencky, E. J. and Goede, A.: Satellite
594 cartography of atmospheric methane from SCIAMACHY on board ENVISAT: 2. Evaluation
595 based on inverse model simulations, *J. Geophys. Res.*, 112, D02304, doi:10.1029/2006JD007268,
596 2007.

597 Bergamaschi, P., Frankenberg, C., Meirink, J. F., Krol, M., Villani, M. G., Houweling, S.,
598 Dentener, F., Dlugokencky, E. J., Miller, J. B., Gatti, L. V., Engel, A. and Levin, I.: Inverse

599 modeling of global and regional CH₄ emissions using SCIAMACHY satellite retrievals, J.
600 Geophys. Res., 114, D22301, doi:10.1029/2009JD012287, 2009.

601 Bergamaschi, P., Houweling, S., Segers, A., Krol, M., Frankenberg, C., Scheepmaker, R. A.,
602 Dlugokencky, E., Wofsy, S. C., Kort, E. a., Sweeney, C., Schuck, T., Brenninkmeijer, C., Chen,
603 H., Beck, V. and Gerbig, C.: Atmospheric CH₄ in the first decade of the 21st century: Inverse
604 modeling analysis using SCIAMACHY satellite retrievals and NOAA surface measurements, J.
605 Geophys. Res. Atmos., 118, 1-20, doi:10.1002/jgrd.50480, 2013.

606 Bey, I., Jacob, D. J., Yantosca, R. M., Logan, J. A., Field, B. D., Fiore, A. M., Li, Q., Liu, H. Y.,
607 Mickley, L. J., and Schultz, M. G.: Global modeling of tropospheric chemistry with assimilated
608 meteorology: model description and evaluation, J. Geophys. Res., 106, 23073-23095, 2001.

609 Bloom, A. A., Palmer, P. I., Fraser, A., Reay, D. S. and Frankenberg, C.: Large-Scale Controls of
610 Methanogenesis Inferred from Methane and Gravity Spaceborne Data, Science, 327, 322–325,
611 doi:10.1038/nchem.467, 2010.

612 Bousquet, P., Ciais, P., Miller, J. B., Dlugokencky, E. J., Hauglustaine, D. A., Prigent, C., Van
613 der Werf, G. R., Peylin, P., Brunke, E.-G., Carouge, C., Langenfelds, R. L., Lathière, J., Papa, F.,
614 Ramonet, M., Schmidt, M., Steele, L. P., Tyler, S. C. and White, J.: Contribution of
615 anthropogenic and natural sources to atmospheric methane variability, Nature, 443(7110), 439–
616 443, doi:10.1038/nature05132, 2006.

617 Bousserez, N., Henze, D. K., Perkins, A., Bowman, K. W., Lee, M., Liu, J., Deng, F. and Jones,
618 D. B. A.: Improved analysis-error covariance matrix for high-dimensional variational inversions:
619 application to source estimation using a 3D atmospheric transport model, Q. J. R. Meteorol. Soc.,
620 doi:10.1002/qj.2495, 2015.

621 Bruhwiler, L. M., Dlugokencky, E., Masarie, K., Ishizawa, M., Andrews, A., Miller, J., Sweeney,
 622 C., Tans, P. and Worthy, D.: CarbonTracker-CH₄: an assimilation system for estimating
 623 emissions of atmospheric methane, *Atmos. Chem. Phys.*, 14, 8269–8293, doi:10.5194/acp-14-
 624 8269-2014, 2014.

625 Butz, A., Hasekamp, O. P., Frankenberg, C., Vidot, J., and Aben, I.: CH₄ retrievals from space-
 626 based solar backscatter measurements: Performance evaluation against simulated aerosol and
 627 cirrus loaded scenes, *J. Geophys. Res. Atmos.*, 115, D24302, doi:10.1029/2010JD014514, 2010.

628 Cressot, C., Chevallier, F., Bousquet, P., Crevoisier, C., Dlugokencky, E. J., Fortems-Cheiney,
 629 A., Frankenberg, C., Parker, R., Pison, I., Scheepmaker, R. A., Montzka, S. A., Krummel, P. B.,
 630 Steele, L. P. and Langenfelds, R. L.: On the consistency between global and regional methane
 631 emissions inferred from SCIAMACHY, TANSO-FTS, IASI and surface measurements, *Atmos.*
 632 *Chem. Phys.*, 14, 577–592, doi:10.5194/acp-14-577-2014, 2014.

633 Deng, F., Jones, D. B. A., Henze, D. K., Bousserez, N., Bowman, K. W., Fisher, J. B., Nassar, R.,
 634 O'Dell, C., Wunch, D., Wennberg, P. O., Kort, E. A., Wofsy, S. C., Blumenstock, T., Deutscher,
 635 N. M., Griffith, D. W. T., Hase, F., Heikkinen, P., Sherlock, V., Strong, K., Sussmann, R. and
 636 Warneke, T.: Inferring regional sources and sinks of atmospheric CO₂ from GOSAT XCO₂ data,
 637 *Atmos. Chem. Phys.*, 14, 3703–3727, doi:10.5194/acp-14-3703-2014, 2014.

638 Denman, K. L., Brasseur, G., Chidthaisong, A., Ciais, P., Cox, P. M., Dickinson, R. E.,
 639 Hauglustaine, D., Heinze, C., Holland, E., Jacob, D., Lohmann, U., Ramachandran, S., da Silva
 640 Dias, P. L., Wofsy, S. C., and Zhang, X.: Couplings Between Changes in the Climate System and
 641 Biogeochemistry. In: *Climate Change 2007: The Physical Science Basis. Contribution of*
 642 *Working Group I to the Fourth Assessment Report of the Intergovernmental Panel on Climate*

643 Change, edited by Solomon, S., Qin, D., Manning, M., Chen, Z., Marquis, M., Averyt, K. B.,
644 Tignor, M., and Miller, H. L., Cambridge University Press, Cambridge, United Kingdom and
645 New York, N. Y., USA, 2007.

646 Dlugokencky, E., Masarie, K. and Lang, P.: Continuing decline in the growth rate of atmospheric
647 methane burden, *Nature*, 393, 447–450, 1998.

648 Dlugokencky, E. J., Houweling, S., Bruhwiler, L., Masarie, K. A., Lang, P. M., Miller, J. B., and
649 Tans, P. P.: Atmospheric methane levels off: Temporary pause or a new steady-state?, *Geophys.*
650 *Res. Lett.*, 30, No. 19, doi: 10.1029/2003GL018126, 2003.

651 Dlugokencky, E. J., Myers, R. C., Lang, P. M., Masarie, K. A., Crotwell, A. M., Thoning, K. W.,
652 Hall, B. D., Elkins, J. W., and Steele, L. P.: Conversion of NOAA atmospheric dry-air CH₄ mole
653 fractions to a gravimetrically prepared standard scale, *J. Geophys. Res. Atmos.*, 110, D18306,
654 doi:10.1029/2005JD006035, 2005.

655 Dlugokencky, E. J., Bruhwiler, L., White, J. W. C., Emmons, L. K., Novelli, P. C., Montzka, S.
656 A., Masarie, K. A., Lang, P. M., Crotwell, A. M., Miller, J. B. and Gatti, L. V.: Observational
657 constraints on recent increases in the atmospheric CH₄ burden, *Geophys. Res. Lett.*, 36, L18803,
658 doi:10.1029/2009GL039780, 2009. Dlugokencky, E. J., Lang, P. M., Crotwell, A. M., Masarie,
659 K. A. and Crotwell M. J.: Atmospheric Methane Dry Air Mole Fractions from the NOAA ESRL
660 Carbon Cycle Cooperative Global Air Sampling Network, 1983-2013, Version: 2014-06-24,
661 ftp://aftp.cmdl.noaa.gov/data/trace_gases/ch4/flask/surface/ (last access: 9 June 2015), 2014.

662 Enting, I. G.: Inverse problems in atmospheric constituent transport, Cambridge University Press,
663 2002.

664 Etheridge, D. M., Steele, L. P., Francey, R. J., and Langenfelds, R. L.: Atmospheric methane
 665 between 1000 A.D. and present: Evidence of anthropogenic emissions and climatic variability, J.
 666 Geophys. Res., 103(D13), 15,979-15,993, 1998.

667 European Commission, Joint Research Centre/Netherlands Environmental Assessment Agency:
 668 Emission Database for Global Atmospheric Research (EDGAR), release version 4.0.,
 669 <http://edgar.jrc.ec.europa.eu> (last access: 11 June 2015), 2009.

670 Fiore, A. M., Horowitz, L. W., Dlugokencky, E. J. and West, J. J.: Impact of meteorology and
 671 emissions on methane trends, 1990–2004, Geophys. Res. Lett., 33, L12809,
 672 doi:10.1029/2006GL026199, 2006.

673 Fisher, R. E., Sriskantharajah, S., Lowry, D., Lanoisellé, M., Fowler, C. M. R., James, R. H.,
 674 Hermansen, O., Lund Myhre, C., Stohl, A., Greinert, J., Nisbet-Jones, P. B. R., Mienert, J. and
 675 Nisbet, E. G.: Arctic methane sources: Isotopic evidence for atmospheric inputs, Geophys. Res.
 676 Lett., 38, L21803, doi:10.1029/2011GL049319, 2011.

677 Frankenberg, C., Meirink, J. F., Bergamaschi, P., Goede, A. P. H., Heimann, M., Kröner, S.,
 678 Platt, U., van Weele, M., and Wagner, T.: Satellite cartography of atmospheric methane from
 679 SCIAMACHY on board ENVISAT: Analysis of the years 2003 and 2004, J. Geophys. Res., 111,
 680 D07303, doi:10.1029/2005JD006235, 2006.

681 Frankenberg, C., Bergamaschi, P., Butz, A., Houweling, S., Meirink, J. F., Notholt, J., Petersen,
 682 A. K., Schrijver, H., Warneke, T., and I. Aben: Tropical methane emissions: A revised view
 683 from SCIAMACHY onboard ENVISAT, Geophys. Res. Lett., 35, L15811,
 684 doi:10.1029/2008GL034300, 2008.

685 Frankenberg, C., Aben, I., Bergamaschi, P., Dlugokencky, E. J., van Hees, R., Houweling, S.,
 686 van der Meer, P., Snel, R., and Tol, P.: Global column-averaged methane mixing ratios from
 687 2003 to 2009 as derived from SCIAMACHY: Trends and variability, *J. Geophys. Res.*, 116,
 688 D02304, doi:10.1029/2010JD014849, 2011.

689 Fraser, A., Palmer, P. I., Feng, L., Boesch, H., Cogan, A., Parker, R., Dlugokencky, E. J., Fraser,
 690 P. J., Krummel, P. B., Langenfelds, R. L., O'Doherty, S., Prinn, R. G., Steele, L. P., van der
 691 Schoot, M. and Weiss, R. F.: Estimating regional methane surface fluxes: the relative importance
 692 of surface and GOSAT mole fraction measurements, *Atmos. Chem. Phys.*, 13, 5697–5713,
 693 doi:10.5194/acp-13-5697-2013, 2013.

694 Fung, I., John, J., Lerner, J., Matthews, E., Prather, M., Steele, L. P., and Fraser, P. J.: Three-
 695 dimensional model synthesis of the global methane cycle, *J. Geophys. Res.*, 96, 13,033–13,065,
 696 doi:10.1029/91JD01247, 1991.

697 GLOBALVIEW-CH4: Cooperative Atmospheric Data Integration Project - Methane. CD-ROM,
 698 NOAA ESRL, Boulder, Colorado, available at: <ftp://ftp.cmdl.noaa.gov> (last access: 19 August
 699 2015), Path: products/globalview/ch4, 2009.

700 Gurney, K. R., Law, R. M., Denning, A. S., Rayner, P. J., Baker, D., Bousquet, P., Bruhwiler, L.,
 701 Chen, Y.-H., Ciais, P., Fan, S., Fung, I. Y., Gloor, M., Heimann, M., Higuchi, K., John, J., Maki,
 702 T., Maksyutov, S., Masarie, K., Peylin, P., Prather, M., Pak, B. C., Randerson, J., Sarmiento, J.,
 703 Taguchi, S., Takahashi, T., and Yuen, C.-W.: Towards robust regional estimates of CO₂ sources
 704 and sinks using atmospheric transport models, *Nature*, 415, 626–630, doi:10.1038/415626a, 2002.

705 Heald, C. L., Jacob, D. J., Jones, D. B. A., Palmer, P. I., Logan, J. A., Streets, D. G., Sachse, G.
 706 W., Gille, J. C., Hoffman, R. N. and Nehrkorn, T.: Comparative inverse analysis of satellite

707 (MOPITT) and aircraft (TRACE-P) observations to estimate Asian sources of carbon monoxide,
 708 J. Geophys. Res., 109, D23306, doi:10.1029/2004JD005185, 2004.

709 Henze, D. K., Hakami, A., and Seinfeld, J. H.: Development of the adjoint of GEOS-Chem,
 710 Atmos. Chem. Phys., 7, 2413–2433, 2007.

711 Houweling, S., Krol, M., Bergamaschi, P., Frankenberg, C., Dlugokencky, E. J., Morino, I.,
 712 Notholt, J., Sherlock, V., Wunch, D., Beck, V., Gerbig, C., Chen, H., Kort, E. a., Röckmann, T.
 713 and Aben, I.: A multi-year methane inversion using SCIAMACHY, accounting for systematic
 714 errors using TCCON measurements, Atmos. Chem. Phys., 14, 3991–4012, doi:10.5194/acp-14-
 715 3991-2014, 2014.

716 Jiang, Z., Jones, D. B. A., Kopacz, M., Liu, J., Henze, D. K., and Heald, C.: Quantifying the
 717 impact of model errors on top-down estimates of carbon monoxide emissions using satellite
 718 observations, J. Geophys. Res., 116, D15306, doi:10.1029/2010JD015282, 2011.

719 Kai, F. M., Tyler, S. C., Randerson, J. T. and Blake, D. R.: Reduced methane growth rate
 720 explained by decreased Northern Hemisphere microbial sources, Nature, 476(7359), 194–197,
 721 doi:10.1038/nature10259, 2011.

722 Kaminski, T. and Heimann, M.: Inverse modeling of atmospheric carbon dioxide fluxes, Science,
 723 294, 259–259, 2001.

724 Keller, C. A., Long, M. S., Yantosca, R. M., Da Silva, A. M., Pawson, S., and Jacob, D. J.:
 725 HEMCO v1.0: a versatile, ESMF-compliant component for calculating emissions in atmospheric
 726 models, Geosci. Model Dev., 7, 1409–1417, doi:10.5194/gmd-7-1409-2014, 2014.

727 Khalil, M. A. K., Butenhoff, C. L. and Rasmussen, R. A.: Atmospheric methane: trends and
 728 cycles of sources and sinks, Environ. Sci. Technol., 41, 2131–2137, 2007.

729 Kim, H., Machida, T., Sasakawa, M., Belikov, D., Saeki, T., Ito, A. and Maksyutov, S.: Recent
730 variation of Siberian CH₄ fluxes estimated from atmospheric observations of CH₄, AGU Fall
731 Meeting Abstracts, 1, GC24A-08, 2012.

732 Kirschke, S., Bousquet, P., Ciais, P., Saunois, M., Canadell, J. G., Dlugokencky, E. J.,
733 Bergamaschi, P., Bergmann, D., Blake, D. R., Bruhwiler, L., Cameron-Smith, P., Castaldi, S.,
734 Chevallier, F., Feng, L., Fraser, A., Heimann, M., Hodson, E. L., Houweling, S., Josse, B., Fraser,
735 P. J., Krummel, P. B., Lamarque, J.-F., Langenfelds, R. L., Le Quéré, C., Naik, V., O'Doherty,
736 S., Palmer, P. I., Pison, I., Plummer, D., Poulter, B., Prinn, R. G., Rigby, M., Ringeval, B.,
737 Santini, M., Schmidt, M., Shindell, D. T., Simpson, I. J., Spahni, R., Steele, L. P., Strode, S. A.,
738 Sudo, K., Szopa, S., van der Werf, G. R., Voulgarakis, A., van Weele, M., Weiss, R. F.,
739 Williams, J. E., and Zeng, G.: Three decades of global methane sources and sinks, *Nat. Geosci.*,
740 6, 813–823, doi:10.1038/ngeo1955, 2013.

741 Kopacz, M., Jacob, D. J., Henze, D. K., Heald, C. L., Streets, D. G. and Zhang, Q.: Comparison
742 of adjoint and analytical Bayesian inversion methods for constraining Asian sources of carbon
743 monoxide using satellite (MOPITT) measurements of CO columns, *J. Geophys. Res.*, 114,
744 D04305, doi:10.1029/2007JD009264, 2009.

745 Kort, E. A., Wofsy, S. C., Daube, B. C., Diao, M., Elkins, J. W., Gao, R. S., Hints, E. J., Hurst,
746 D. F., Jimenez, R., Moore, F. L., Spackman, J. R. and Zondlo, M. A.: Atmospheric observations
747 of Arctic Ocean methane emissions up to 82° north, *Nat. Geosci.*, 5, 1–4, doi:10.1038/ngeo1452,
748 2012.

749 Koven, C. D., Ringeval, B., Friedlingstein, P., Ciais, P., Cadule, P., Khvorostyanov, D., Krinner,
 750 G. and Tarnocai, C.: Permafrost carbon-climate feedbacks accelerate global warming, *Proc. Natl.*
 751 *Acad. Sci.*, 108, 14769–14774, doi:10.1073/pnas.1103910108, 2011.

752 Langenfelds, R. L., Francey, R. J., Pak, B. C., Steele, L. P., Lloyd, J., Trudinger, C. M. and
 753 Allison, C. E.: Interannual growth rate variations of atmospheric CO₂ and its $\delta^{13}\text{C}$, H₂, CH₄, and
 754 CO between 1992 and 1999 linked to biomass burning, *Global Biogeochem. Cycles*, 16(3), 1048,
 755 doi:10.1029/2001GB001466, 2002.

756 Lehner, B. and Döll, P.: Development and validation of a global database of lakes, reservoirs and
 757 wetlands, *J. Hydrol.*, 296, 1–22, 2004.

758 Levin, I., Veidt, C., Vaughn, B. H., Brailsford, G., Bromley, T., Heinz, R., Lowe, D., Miller, J.
 759 B., Poß, C. and White, J. W. C.: No inter-hemispheric $\delta^{13}\text{CH}_4$ trend observed, *Nature*, 486, E3–
 760 E4, doi:10.1038/nature11175, 2012.

761 Lin, S.-J. and Rood, R. B.: Multidimensional Flux-Form Semi-Lagrangian Transport Schemes,
 762 *Mon. Weather Rev.*, 124, 2046–2070, 1996.

763 Lu, X. and Zhuang, Q.: Modeling methane emissions from the Alaskan Yukon River basin,
 764 1986–2005, by coupling a large-scale hydrological model and a process-based methane model, *J.*
 765 *Geophys. Res.*, 117, G02010, doi:10.1029/2011JG001843, 2012.

766 Machida, T., Nakazawa, T., Muksyutov, S., Tohjima, Y., Takahashi, Y., Watai, T., Vinnichenko,
 767 N., Panchenko, M., Arshinov, M., Fedoseev, N., and Inoue, G.: Temporal and spatial variations
 768 of atmospheric CO₂ mixing ratio over Siberia, paper presented at the Sixth International CO₂
 769 Conference, Sendai, Japan, 1–5, 2001.

770 McGuire, A. D., Christensen, T. R., Hayes, D., Herault, A., Euskirchen, E., Kimball, J. S.,
 771 Koven, C., Lafleur, P., Miller, P. A., Oechel, W., Peylin, P., Williams, M., and Yi, Y.: An
 772 assessment of the carbon balance of Arctic tundra: comparisons among observations, process
 773 models, and atmospheric inversions, *Biogeosciences*, 9, 3185–3204, doi:10.5194/bg-9-3185-2012,
 774 2012.

775 Meirink, J. F., Bergamaschi, P. and Krol, M. C.: Four-dimensional variational data assimilation
 776 for inverse modelling of atmospheric methane emissions: method and comparison with synthesis
 777 inversion, *Atmos. Chem. Phys.*, 8, 6341–6353, doi:10.5194/acp-8-6341-2008, 2008.

778 Melton, J. R., et al.: Present state of global wetland extent and wetland methane modelling:
 779 conclusions from a model inter-comparison project (WETCHIMP), *Biogeosciences*, 10, 753–788,
 780 2013.

781 Meng, L., Paudel, R., Hess, P. G. M. and Mahowald, N. M.: Seasonal and interannual variability
 782 in wetland methane emissions simulated by CLM4Me' and CAM-chem and comparisons to
 783 observations of concentrations, *Biogeosciences*, 12, 4029–4049, doi:10.5194/bg-12-4029-2015,
 784 2015.

785 Miller, S. M., Wofsy, S. C., Michalak, A. M., Kort, E. A., Andrews, A. E., Biraud, S. C.,
 786 Dlugokencky, E. J., Eluszkiewicz, J., Fischer, M. L., Janssens-Maenhout, G., Miller, B. R.,
 787 Miller, J. B., Montzka, S. A., Nehrkorn, T. and Sweeney, C.: Anthropogenic emissions of
 788 methane in the United States, *Proc. Natl. Acad. Sci.*, 110(50), 20018–20022,
 789 doi:10.1073/pnas.1314392110, 2013.

790 Miller, S. M., Worthy, D. E. J., Michalak, A. M., Wofsy, S. C., Kort, E. A., Havice, T. C.,
 791 Andrews, A. E., Dlugokencky, E. J., Kaplan, J. O., Levi, P. J., Tian, H. and Zhang, B.:

792 Observational constraints on the distribution, seasonality, and environmental predictors of North
 793 American boreal methane emissions, *Global Biogeochem. Cycles*, 28, 146–160,
 794 doi:10.1002/2013GB004580, 2014.

795 Miyazaki, K., Patra, P. K., Takigawa, M., Iwasaki, T. and Nakazawa, T.: Global-scale transport
 796 of carbon dioxide in the troposphere, *J. Geophys. Res.*, 113, D15301,
 797 doi:10.1029/2007JD009557, 2008.

798 Monteil, G., Houweling, S., Butz, A., Guerlet, S., Schepers, D., Hasekamp, O., Frankenberg, C.,
 799 Scheepmaker, R., Aben, I. and Röckmann, T.: Comparison of CH₄ inversions based on 15
 800 months of GOSAT and SCIAMACHY observations, *J. Geophys. Res. Atmos.*, 118, 1–17,
 801 doi:10.1002/2013JD019760, 2013.

802 Murray, L. T., Jacob, D. J., Logan, J. A., Hudman, R. C., and Koshak, W. J.: Optimized regional
 803 and interannual variability of lightning in a global chemical transport model constrained by
 804 LIS/OTD satellite data, *J. Geophys. Res.*, 117, D20307, doi:10.1029/2012JD017934, 2012.

805 Myhre, G., Shindell, D., Bréon, F.-M., Collins, W., Fuglestad, J., Huang, J., Koch, D.,
 806 Lamarque, J.-F., Lee, D., Mendoza, B., Nakajima, T., Robock, A., Stephens, G., Takemura, T.,
 807 and Zhang, H.: Anthropogenic and natural radiative forcing, in: *Climate Change 2013: the*
 808 *Physical Science Basis*, contribution of Working Group I to the Fifth Assessment Report of the
 809 Intergovernmental Panel on Climate Change, edited by: Stocker, T. F., Qin, D., Plattner, G.-K.,
 810 Tignor, M., Allen, S. K., Boschung, J., Nauels, A., Xia, Y., Bex, V., and Midgley, P. M.,
 811 Cambridge University Press, Cambridge, UK and New York, NY, USA, 2013.

812 [Myhre, C. L., Ferré, B., Platt, S. M., Silyakova, A., Hermansen, O., Allen, G., Pissó, I.,](#)
 813 [Schmidbauer, N., Stohl, A., Pitt, J., Jansson, P., Greinert, J., Percival, C., Fjaeraa, A. M., O’Shea,](#)

[S., Gallagher, M., Le Breton, M., Bower, K., Bauguitte, S., Dalsøren, S., Vadakkepuliambatta, S., Fisher, R. E., Nisbet, E. G., Lowry, D., Myhre, G., Pyle, J., Cain, M. and Mienert, J.: Extensive release of methane from Arctic seabed west of Svalbard during summer 2014 does not influence the atmosphere, *Geophys. Res. Lett.*, 43, 4624–4631, doi:10.1002/2016GL068999, 2016.](#)

Nisbet, E. G., Dlugokencky, E. J. and Bousquet, P.: Methane on the Rise--Again, *Science*, 343, 493–495, doi:10.1126/science.1247828, 2014.

Oh, Y., Stackhouse, B., Lau, M. C. Y., Xu, X., Trugman, A. T., Moch, J., Onstott, T. C., Jørgensen, C. J., Ludovica, D., Elberling, B., Emmerton, C. A., St. Louis, V. L. and Medvigy, D.: A scalable model explaining methane consumption in arctic mineral soils, *Geophys. Res. Lett.*, 43, 5143–5150, doi:10.1002/2016GL069049, 2016.

Park, R. J., Jacob, D. J., Field, B. D., Yantosca, R. M., and Chin, M.: Natural and transboundary pollution influences on sulfate-nitrate-ammonium aerosols in the United States: Implications for policy, *J. Geophys. Res.*, 109, D15204, doi:10.1029/2003JD004473, 2004.

Parker, R., Boesch, H., Cogan, A., Fraser, A., Feng, L., Palmer, P. I., Messerschmidt, J., Deutscher, N., Griffith, D. W. T., Notholt, J., Wennberg, P. O., and Wunch, D.: Methane observations from the Greenhouse Gases Observing SATellite: Comparison to ground-based TCCON data and model calculations, *Geophys. Res. Lett.*, 38, L15807, doi:10.1029/2011GL047871, 2011.

Peng, S. S., Piao, S. L., Bousquet, P., Ciais, P., Li, B. G., Lin, X., Tao, S., Wang, Z. P., Zhang, Y., and Zhou, F.: Inventory of anthropogenic methane emissions in Mainland China from 1980 to 2010, *Atmos. Chem. Phys. Discuss.*, doi:10.5194/acp-2016-139, in review, 2016.

836 Pickett-Heaps, C. A., Jacob, D. J., Wecht, K. J., Kort, E. A., Wofsy, S. C., Diskin, G. S., Worthy,
837 D. E. J., Kaplan, J. O., Bey, I., and Drevet, J.: Magnitude of seasonality of wetland methane
838 emissions from the Hudson Bay Lowlands (Canada), *Atmos. Chem. Phys.*, 11, 3773–3779,
839 doi:10.5194/acp-11-3773-2011, 2011.

840 Prather, M. J., Holmes, C. D., and Hsu, J.: Reactive greenhouse gas scenarios: systematic
841 exploration of uncertainties and the role of atmospheric chemistry, *Geophys. Res. Lett.*, 39,
842 L09803, doi:10.1029/2012gl051440, 2012.

843 Rigby, M., Prinn, R. G., Fraser, P. J., Simmonds, P. G., Langenfelds, R. L., Huang, J., Cunnold,
844 D. M., Steele, L. P., Krummel, P. B., Weiss, R. F., O'Doherty, S., Salameh, P. K., Wang, H. J.,
845 Harth, C. M., Mühle, J. and Porter, L. W.: Renewed growth of atmospheric methane, *Geophys.*
846 *Res. Lett.*, 35, L22805, doi:10.1029/2008GL036037, 2008.

847 Rodgers, C. D.: *Inverse Methods for Atmospheric Sounding: Theory and Practice*, Vol. 2, edited
848 by: Rodgers, C. D., World Scientific Publishing Co. Pte. Ltd., Singapore, 2000.

849 Saarnio, S., Winiwarter, W. and Leitão, J.: Methane release from wetlands and watercourses in
850 Europe, *Atmos. Environ.*, 43, 1421–1429, doi:10.1016/j.atmosenv.2008.04.007, 2009.

851 Sasakawa, M., Machida, T., Tsuda, N., Arshinov, M., Davydov, D., Fofonov, A. and Krasnov,
852 O.: Aircraft and tower measurements of CO₂ concentration in the planetary boundary layer and
853 the lower free troposphere over southern taiga in West Siberia: Long-term records from 2002 to
854 2011, *J. Geophys. Res.*, 118, 9489–9498, doi:10.1002/jgrd.50755, 2013.

855 Schubert, C. J., Diem, T. and Eugster, W.: Methane Emissions from a Small Wind Shielded Lake
 856 Determined by Eddy Covariance, Flux Chambers, Anchored Funnels, and Boundary Model
 857 Calculations: A Comparison, Environ. Sci. Technol., 46, 4515–4522, 2012.

858 Schuur, E. A. G., McGuire, A. D., Schädel, C., Grosse, G., Harden, J. W., Hayes, D. J., Hugelius,
 859 G., Koven, C. D., Kuhry, P., Lawrence, D. M., M.Natali, S., Olefeldt, D., Romanovsky, V. E.,
 860 Schaefer, K., Turetsky, M. R., Treat, C. C. and Vonk, E. J.: Climate change and the permafrost
 861 carbon feedback, Nature, 520, 171–179, doi:10.1038/nature14338, 2015.

862 ~~Shakhova, N., Semiletov, I., Leifer, I., Sergienko, V., Salyuk, A., Kosmach, D., Chernykh, D.,~~
 863 ~~Stubbs, C., Nicolsky, D., Tumskey, V. and Gustafsson, Ö.: Ebullition and storm-induced~~
 864 ~~methane release from the East Siberian Arctic Shelf, Nat. Geosci., 7, doi:10.1038/ngeo2007,~~
 865 ~~2013.~~

866 Shindell, D. T., Faluvegi, G., Koch, D. M., Schmidt, G. A., Unger, N., and Bauer, S. E.:
 867 Improved attribution of climate forcing to emissions, Science, 326, 716-718, 2009.

868 Simpson, I. J., Sulbaek Andersen, M. P., Meinardi, S., Bruhwiler, L., Blake, N. J., Helmig, D.,
 869 Rowland, F. S. and Blake, D. R.: Long-term decline of global atmospheric ethane concentrations
 870 and implications for methane, Nature, 488, 490–494, doi:10.1038/nature11342, 2012.

871 Singh, K., Jardak, M., Sandu, A., Bowman, K., Lee, M., and Jones, D.: Construction of non-
 872 diagonal background error covariance matrices for global chemical data assimilation, Geosci.
 873 Model Dev., 4, 299-316, 2011.

874 Sweeney, C., Karion, A., Wolter, S., Newberger, T., Guenther, D., Higgs, J. A., Andrews, A. E.,
 875 Lang, P. M., Neff, D., Dlugokencky, E., Miller, J. B., Montzka, S. A., Miller, B. R., Masarie, K.
 876 A., Biraud, S. A., Novelli, P. C., Crotwell, M., Crotwell, A. M., Thoning, K. and Tans, P. P.:

877 Seasonal climatology of CO₂ across North America from aircraft measurements in the
878 NOAA/ESRL Global Greenhouse Gas Reference Network, *J. Geophys. Res. Atmos.*, 120, 5155–
879 5190, doi:10.1002/2014JD022591, 2015.

880 Tan, Z., Zhuang, Q. and Walter Anthony, K.: Modeling methane emissions from arctic lakes:
881 Model development and site-level study, *J. Adv. Model. Earth Syst.*, 7, 459-483,
882 doi:10.1002/2014MS000314, 2015.

883 Tan, Z. and Zhuang, Q.: Arctic lakes are continuous methane sources to the atmosphere under
884 warming conditions, *Environ. Res. Lett.*, 10, 054016, doi:10.1088/1748-9326/10/5/054016,
885 2015a.

886 Tan, Z. and Zhuang, Q.: Methane emissions from pan-Arctic lakes during the 21st century: An
887 analysis with process-based models of lake evolution and biogeochemistry, *J. Geophys. Res.*
888 *Biogeosciences*, 120, 2641–2653, doi:10.1002/2015JG003184, 2015b.

889 Tarnocai, C., Canadell, J. G., Schuur, E. A. G., Kuhry, P., Mazhitova, G. and Zimov, S.: Soil
890 organic carbon pools in the northern circumpolar permafrost region, *Global Biogeochem. Cycles*,
891 23, GB2023, doi: 10.1029/2008GB003327, 2009.

892 Thompson, R. L., Stohl, A., Zhou, L. X., Dlugokencky, E., Fukuyama, Y., Tohjima, Y., Kim, S.-
893 Y., Lee, H., Nisbet, E. G., Fisher, R. E., Lowry, D., Weiss, R. F., Prinn, R. G., O'Doherty, S.,
894 Young, D. and White, J. W. C.: Methane emissions in East Asia for 2000 – 2011 estimated using
895 atmospheric Bayesian inversion, *J. Geophys. Res. Atmos.*, 120, 4352–4369,
896 | doi:10.1002/2014JD022394, 2015.

897 [Thornton, B. F., Geibel, M. C., Crill, P. M., Humborg, C. and Mörrth, C.-M.: Methane fluxes](#)
 898 [from the sea to the atmosphere across the Siberian shelf seas, *Geophys. Res. Lett.*, 43, 5869–](#)
 899 [5877, doi:10.1002/2016GL068977, 2016.](#)

900 Turner, A. J., Jacob, D. J., Wecht, K. J., Maasakkers, J. D., Biraud, S. C., Boesch, H., Bowman,
 901 K. W., Deutscher, N. M., Dubey, M. K., Griffith, D. W. T., Hase, F., Kuze, A., Notholt, J.,
 902 Ohyama, H., Parker, R., Payne, V. H., Sussmann, R., Velasco, V. A., Warneke, T., Wennberg, P.
 903 O. and Wunch, D.: Estimating global and North American methane emissions with high spatial
 904 resolution using GOSAT satellite data, *Atmos. Chem. Phys.*, 15, 7049–7069, doi:10.5194/acp-
 905 15-7049-2015, 2015.

906 van der Werf, G. R., Randerson, J. T., Giglio, L., Collatz, G. J., Mu, M., Kasibhatla, P. S.,
 907 Morton, D. C., DeFries, R. S., Jin, Y., and van Leeuwen, T. T.: Global fire emissions and the
 908 contribution of deforestation, savanna, forest, agricultural, and peat fires (1997–2009), *Atmos.*
 909 *Chem. Phys.*, 10, 11,707–11,735, doi:10.5194/acp-10-11707-2010, 2010.

910 Walter, K. M., Zimov, S. A., Chanton, J. P., Verbyla, D. and Chapin III, F. S.: Methane bubbling
 911 from Siberian thaw lakes as a positive feedback to climate warming, *Nature*, 443, 71–75,
 912 doi:10.1038/nature05040, 2006.

913 Walter, K. M., Smith, L. C. and Chapin III, F. S.: Methane bubbling from northern lakes: present
 914 and future contributions to the global methane budget, *Philos. T. Roy. Soc. A*, 365(1856), 1657–
 915 76, doi:10.1098/rsta.2007.2036, 2007.

916 Wania, R., Melton, J. R., Hodson, E. L., Poulter, B., Ringeval, B., Spahni, R., Bohn, T., Avis, C.
 917 A., Chen, G., Eliseev, A. V., Hopcroft, P. O., Riley, W. J., Subin, Z. M., Tian, H., van Bodegom,
 918 P. M., Kleinen, T., Yu, Z. C., Singarayer, J. S., Zürcher, S., Lettenmaier, D. P., Beerling, D. J.,

919 Denisov, S. N., Prigent, C., Papa, F. and Kaplan, J. O.: Present state of global wetland extent and
 920 wetland methane modelling: methodology of a model inter-comparison project (WETCHIMP),
 921 *Geosci. Model Dev.*, 6, 617–641, doi:10.5194/gmd-6-617-2013, 2013.

922 Wang, J. S., Logan, J. L., McElroy, M. B., Duncan, B. N., Megretskaya, I. A., and Yantosca, R.
 923 M.: 3-D model analysis of the slowdown and interannual variability in the methane growth rate
 924 from 1988 to 1997, *Global Biogeochem. Cycles*, 18, GB3011, doi:10.1029/2003GB002180,
 925 2004.

926 Wecht, K. J., Jacob, D. J., Frankenberg, C., Jiang, Z. and Blake, D. R.: Mapping of North
 927 American methane emissions with high spatial resolution by inversion of SCIAMACHY satellite
 928 data, *J. Geophys. Res. Atmos.*, 119, 7741–7756, doi:10.1002/2014JD021551, 2014.

929 Zhu, X., Zhuang, Q., Qin, Z., Glagolev, M. and Song, L.: Estimating wetland methane emissions
 930 from the northern high latitudes from 1990 to 2009 using artificial neural networks, *Global*
 931 *Biogeochem. Cycles*, 27, 1–13, doi:10.1002/gbc.20052, 2013.

932 Zhuang, Q., Melillo, J. M., Kicklighter, D. W., Prinn, R. G., McGuire, A. D., Steudler, P. A.,
 933 Felzer, B. S., and Hu, S.: Methane fluxes between terrestrial ecosystems and the atmosphere at
 934 northern high latitudes during the past century: A retrospective analysis with a process-based
 935 biogeochemistry model, *Global Biogeochem. Cycles*, 18, GB3010, doi:10.1029/2004GB002239,
 936 2004.

937 Zhuang, Q., Melillo, J. M., Sarofim, M. C., Kicklighter, D. W., McGuire, a. D., Felzer, B. S.,
 938 Sokolov, A., Prinn, R. G., Steudler, P. a. and Hu, S.: CO₂ and CH₄ exchanges between land
 939 ecosystems and the atmosphere in northern high latitudes over the 21st century, *Geophys. Res.*
 940 *Lett.*, 33, L17403, doi:10.1029/2006GL026972, 2006.

Zhuang, Q., Melillo, J. M., McGuire, A. D., Kicklighter, D. W., Prinn, R. G., Steudler, P. A., Felzer, B. S. and Hu, S.: Net emissions of CH₄ and CO₂ in Alaska: Implications for the region's greenhouse gas budget, *Ecol. Appl.*, 17, 203–212, 2007.

Figure Captions

Figure 1. SCIAMACHY retrievals ($n = 37743$) of the weighted column-average CH₄ dry mole fractions for July 2005–September 2005 in the pan-Arctic that have passed all quality control tests described in Section 2.1 and the locations of surface flask stations and aircraft missions used for data assimilation or inversion evaluation.

Figure 2. Prior average CH₄ fluxes from wetlands, lakes and other sources (i.e. anthropogenic and biomass burning) in 2005 used for the pan-Arctic nested grid inversions at $1/2^\circ \times 2/3^\circ$ resolution. Annual total emission for each pan-Arctic source is presented in units of Tg CH₄ yr⁻¹.

Figure 3. Bias correction function (left) and standard deviation (right) for SCIAMACHY retrievals overpassing the pan-Arctic. ΔXCH_4 is the difference between SCIAMACHY and column-average mixing ratios mapped from aircraft vertical profiles. The red line in the left shows a linear regression weighted by the number of SCIAMACHY retrievals.

Figure 4. Optimized pan-Arctic CH₄ fluxes in 2005 at $1/2^\circ \times 2/3^\circ$ resolution using both SCIAMACHY and NOAA/ESRL observations. a) BERN; b) CLM4Me; c) DLEM; d) ORCHIDEE; e) SDGVM; f) WSL.

Figure 5. Comparison of prior and posterior pan-Arctic CH₄ emissions and their uncertainties. “NOAA only” represents posterior emissions assimilating only surface measurements. “NOAA + SCIA” represents posterior emissions assimilating both surface measurements and satellite

retrievals. The uncertainty of prior emissions is 100%. Scenarios are represented by their name initials: “B” for BERN, “C” for CLM4Me, “D” for DLEM, “O” for ORCHIDEE, “S” for SDGVM and “W” for WSL.

Figure 6. Distribution of the relative difference between the observed and simulated posterior SCIAMACHY column-average mixing ratios. The “DLEM + Lake” scenario includes CH₄ emissions from both wetlands and lakes and the “DLEM only” scenario only includes CH₄ emissions from wetlands. Relative difference is calculated as a percentage of absolute

differences between GEOS-Chem and SCIAMACHY relative to SCIAMACHY retrievals. [Two extending red and blue lines represent the means of the simulation bias under the “DLEM + Lake” scenario and the “DLEM only” scenario, respectively.](#)

Figure 7. Evaluation of the posterior GEOS-Chem CH₄ mole fractions from the pan-Arctic nested-grid inversions with independent data sets from the NOAA flask stations, the NOAA aircraft PFA profiles and the NIES aircraft Surgut profiles. Black symbols indicate the rms of the forward GEOS-Chem runs and red symbols indicate the rms of the global inversions.

Table1. Summary of bias correction methods and of mean absolute satellite-model difference (ppb) for 2003-2005 before and after applying bias correction. ΔBIC is the BIC score increase of a bias correction method when referring to the latitude only method.

	Bias correction function [*]	Mean absolute difference	ΔBIC	R^2
No correction		9.271		
Latitude only	$p_0 + p_1\varphi + p_2\varphi^2$	6.305		0.62
Air mass factor only	$p_0 + p_1A_F$	7.071	161	0.52
Humidity only	$p_0 + p_1H_S$	6.786	73	0.56
Latitude + Humidity	$p_0 + p_{11}\varphi + p_{12}\varphi^2 + p_{21}H_S$	6.230	-7	0.62
Air mass factor + Humidity	$p_0 + p_{11}A_F + p_{21}H_S$	6.396	12	0.60

^{*} p_0 , p_1 , p_2 , p_{11} , p_{12} and p_{21} are regression parameters.

Table 2. Estimated annual CH₄ emissions (units: Tg CH₄ yr⁻¹) for TransCom 3 land regions (NAB: North American Boreal, NAT: North American Temperate, SATr: South American Tropical, SAT: South American Temperate, NAF: Northern Africa, SAF: Southern Africa, ErB: Eurasian Boreal, ErT: Eurasian Temperate, TrA: Tropical Asia, Aus: Australasia, and Eur: Europe). The priors are the range of the initial CH₄ emissions given by the six scenarios.

Region	Priors	Posterior						Fraser et al. (2013)	Alexe et al. (2015)
		Bern	CLM4Me	DLEM	ORCHIDEE	SDGVM	WSL		
NAB	7.9–26.0	24.3	16.2	16.8	27.4	12.0	20.7	5.1±1.1	10.3
NAT	38.5–59.2	33.2	32.8	42.8	49.2	51.2	39.7	62.5±4.4	45.6
SATr	29.6–100.0	43.0	60.8	31.4	61.0	62.3	42.1	49.6±6.4	71.8
SAT	29.1–55.8	31.2	27.1	35.2	39.1	25.6	30.5	55.8±9.5	40.2
NAf	26.8–31.2	34.0	41.3	27.9	28.0	27.7	32.0	46.9±7.3	50.6
SAf	16.0–27.0	18.4	16.2	19.0	24.2	15.6	18.7	36.6±5.8	42.0
ErB	11.5–32.7	19.2	14.3	16.5	18.7	22.2	14.9	16.5±3.8	15.4
ErT	114.9–133.5	97.0	84.9	146.1	92.7	98.3	99.8	115.9±7.3	109.6
TrA	33.1–45.8	47.3	51.4	35.8	33.1	36.4	45.1	43.5±3.2	76.8
Aus	5.8–8.3	7.3	7.7	6.6	7.9	6.3	7.3	17.6±2.7	4.3
Eur	43.6–53.5	54.9	52.2	46.4	43.5	56.5	54.1	39.6±3.7	28.9
Wetlands	121.7–278.1	166.8	164.6	130.0	203.3	161.8	160.7	192.1±16.1	169
Global	471.5–627.8	501.0	497.7	511.5	511.0	496.4	502.9	510.6±18.4	540.5

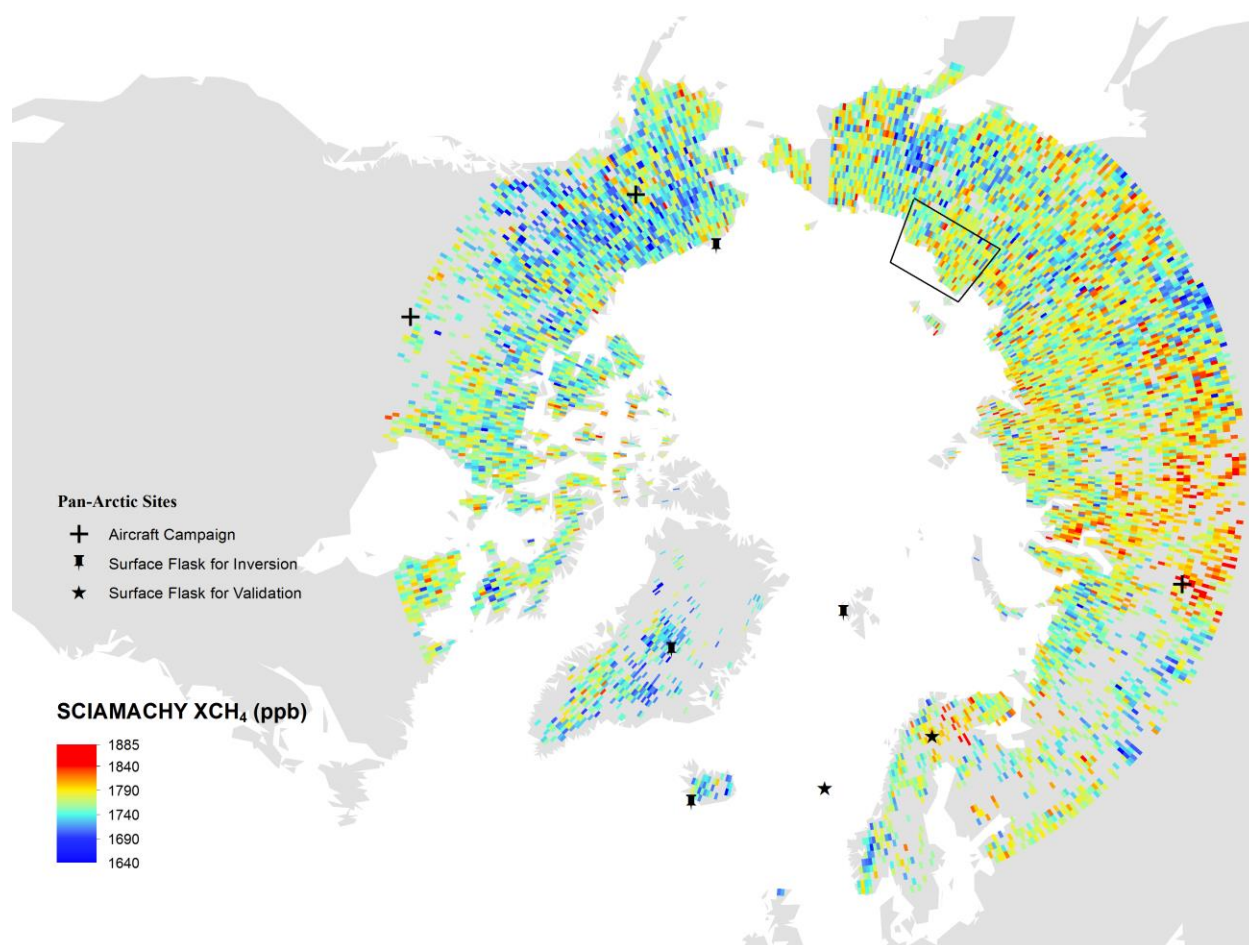


Figure 1.

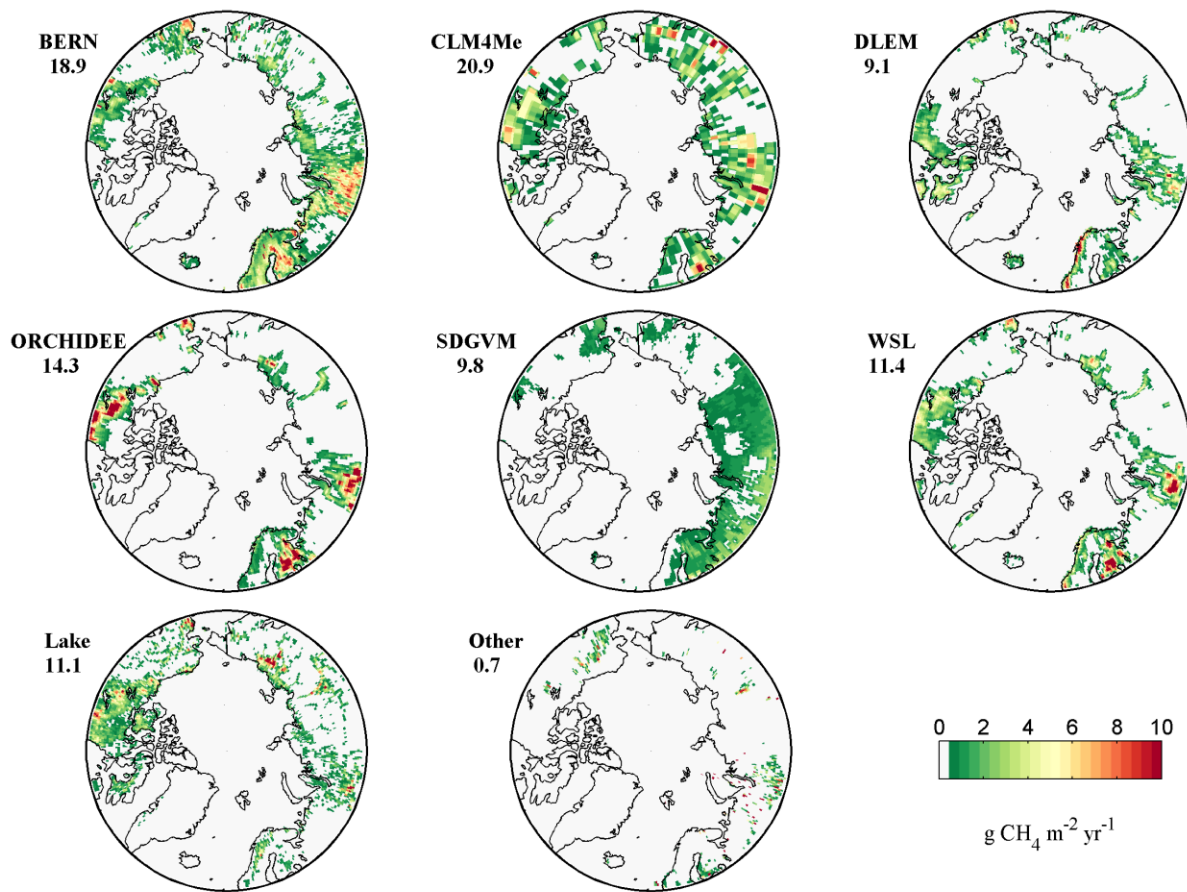


Figure 2.

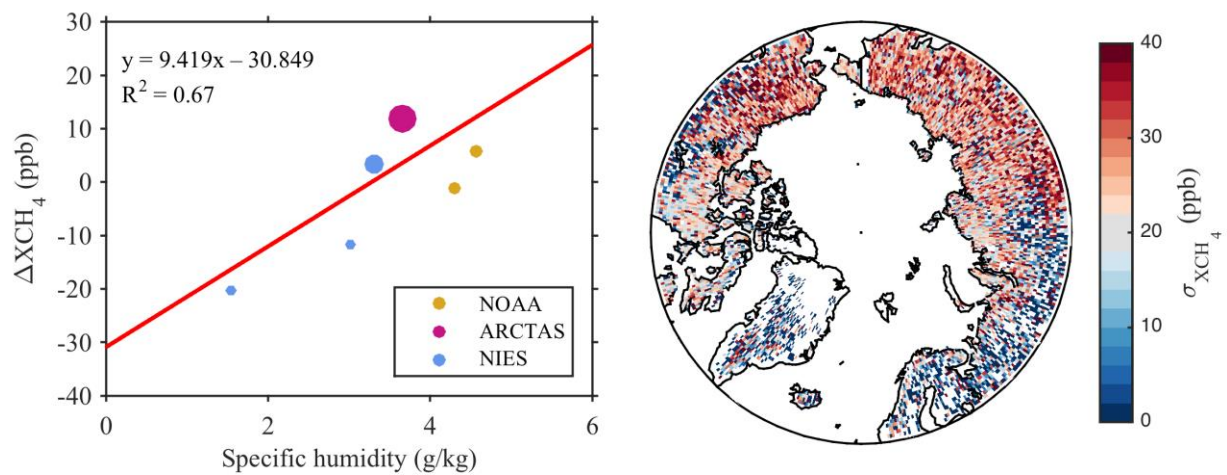


Figure 3.

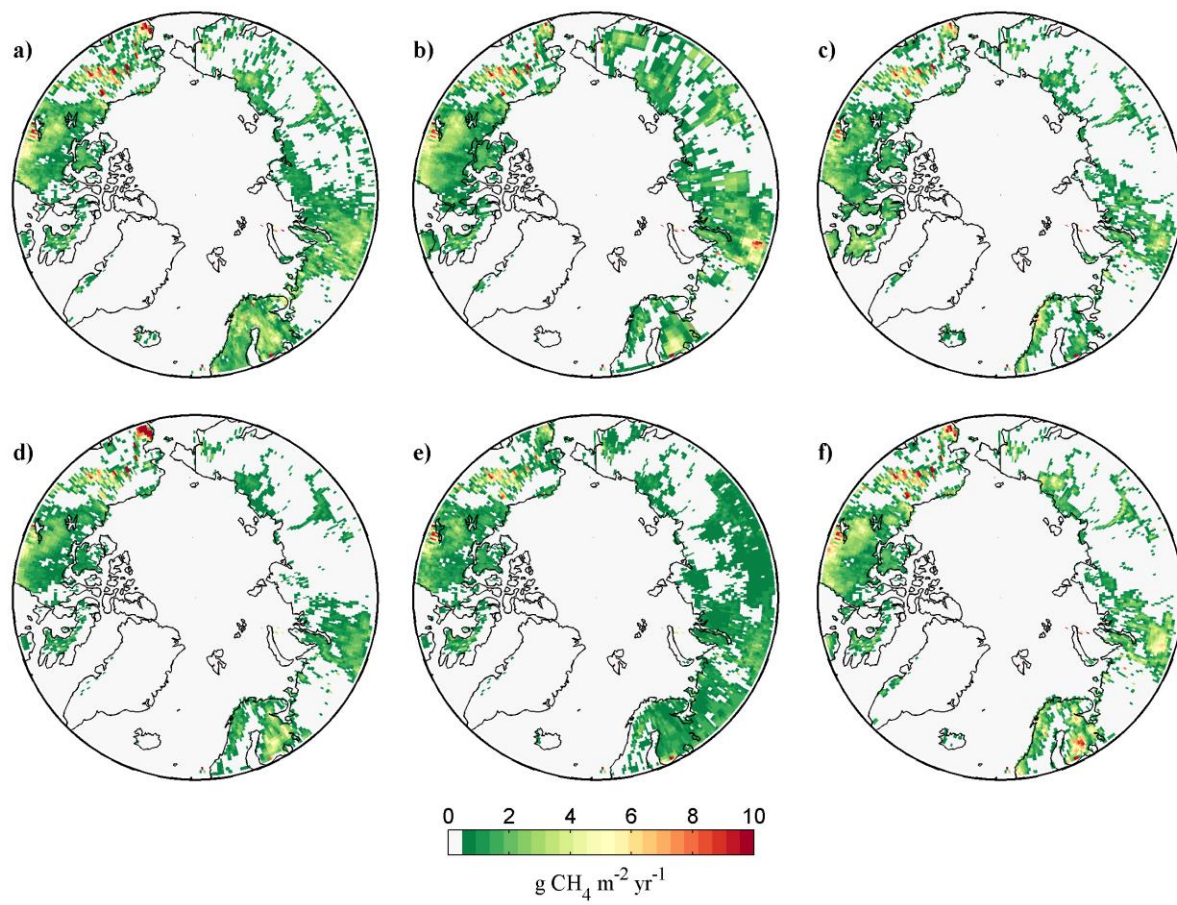


Figure 4.

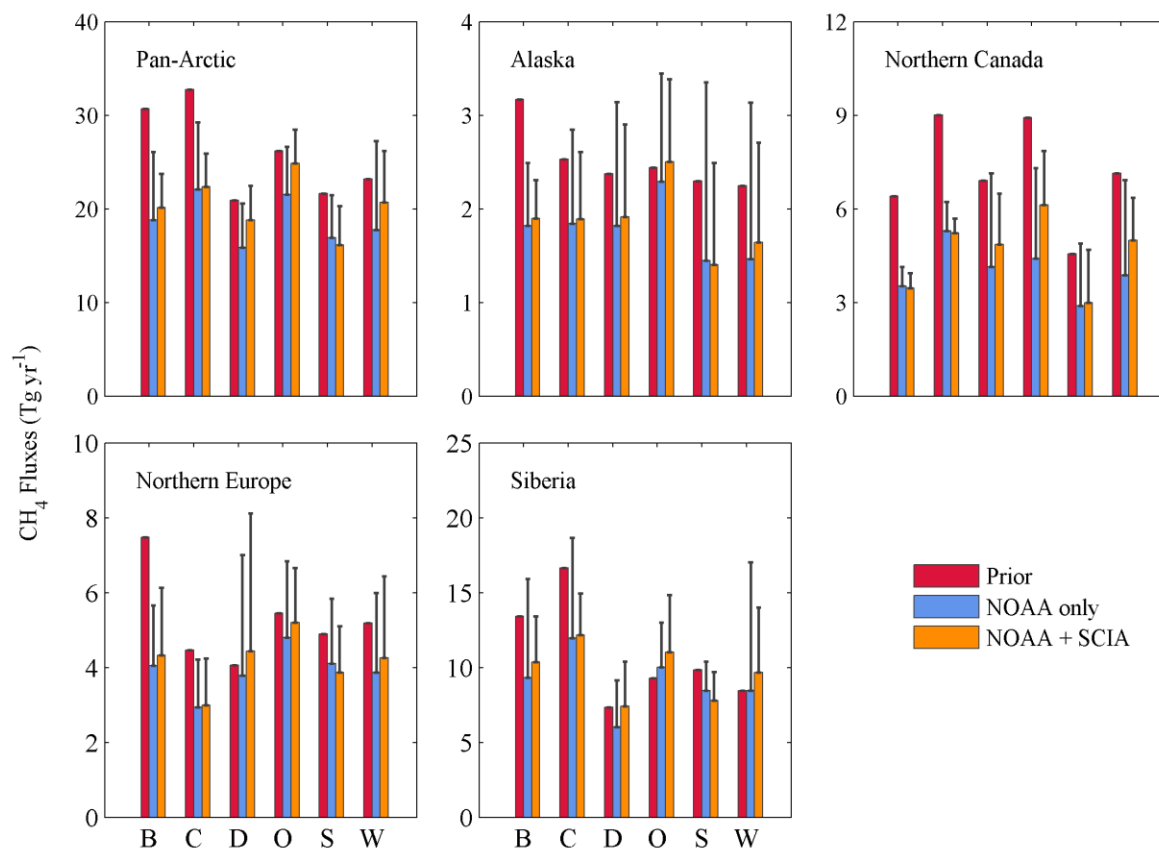
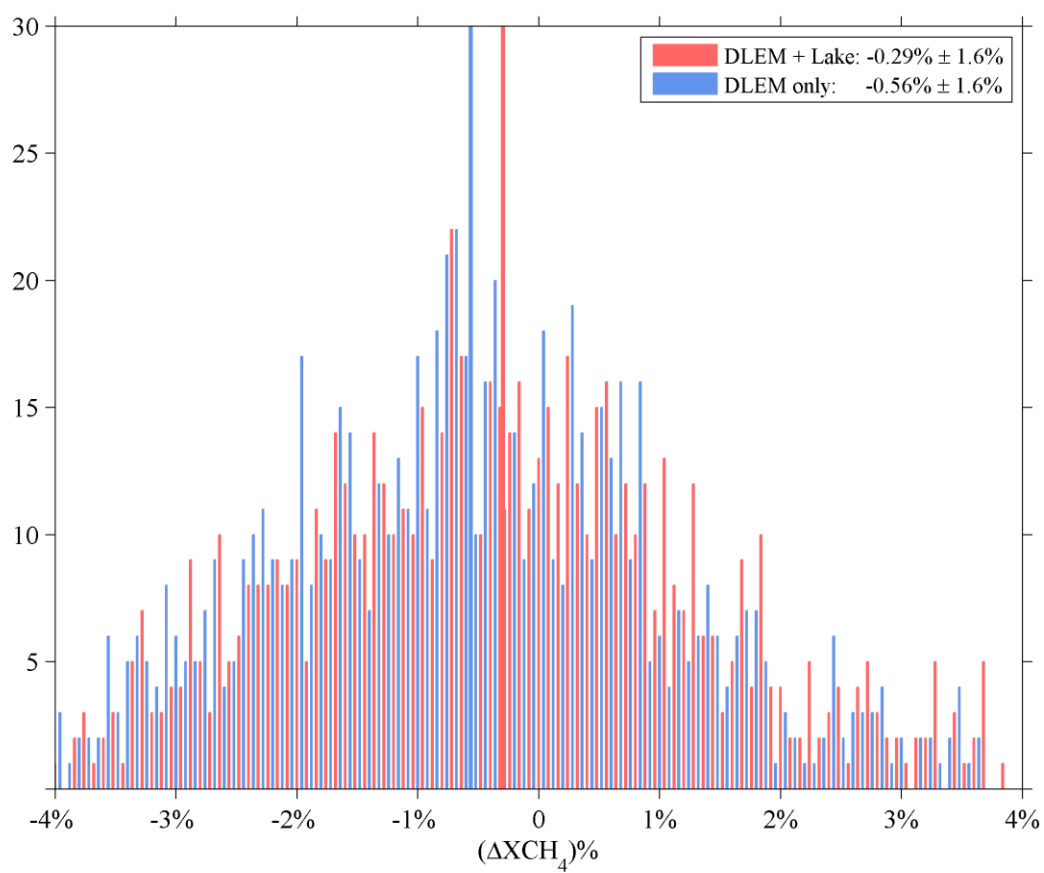


Figure 5.



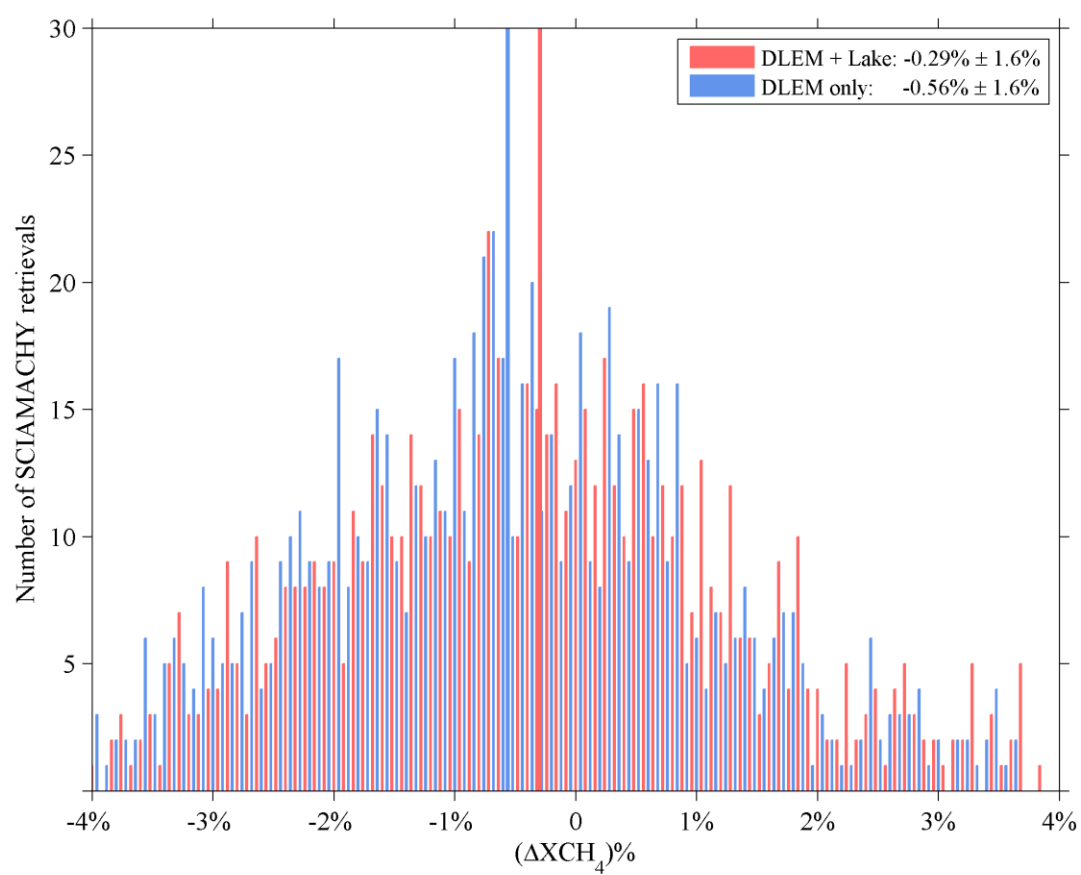


Figure 6.

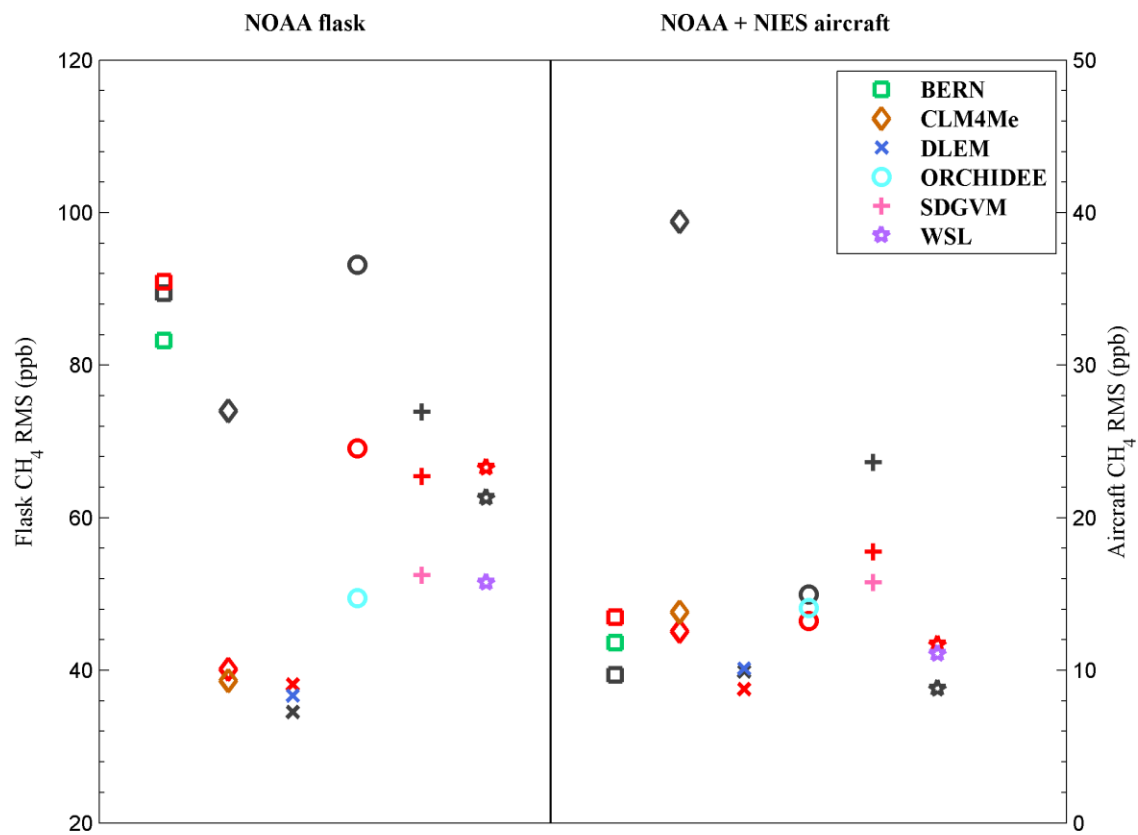


Figure 7.

S1. Methods and Results

In the text S1, the steps to construct optimal initial conditions for global and nested grid inversions are described. We also describe the steps to construct an optimal GEOS-Chem CH₄ field for SCIAMACHY bias correction purpose and the comparison between our estimates and previous inversion studies in the global scale.

To start global and nested-grid inversions, the initial CH₄ field of the GEOS-Chem model needs to be optimized to minimize its error. As our focus is in the period of 2004–2005, to speed up the whole process, we only ran one inversion from 1993 to 2003 using the LPJ-WSL scenario and NOAA/ESRL measurements. The main purpose of this inversion is to construct initial CH₄ field in 2004. As presented in Fig. S2, without optimization, the LPJ-WSL scenario gives the best fit of the GEOS-Chem modeled CH₄ to the GLOBALVIEW-CH₄ data (GLOBALVIEW-CH₄, 2009). During the 1993–2003 inversion, GEOS-Chem was driven by GEOS-4 meteorological (met) data from NASA’s Global Modeling Assimilation Office (GMAO). Relative to GEOS-5, the GEOS-4 met data has the same horizontal resolutions but less vertical hybrid sigma-pressure levels (55 vertical levels).

To construct optimal atmospheric CH₄ fields for the bias correction of SCIAMACHY retrievals at the global scale, we ran a global inversion during 2004–2005 using the LPJ-WSL wetland emission scenario and NOAA/ESRL measurements. In this inversion, the GEOS-Chem model was driven by the GEOS-5 met data. The global inversions of different scenarios that assimilated both surface measurements and satellite retrievals were then run in two sequential time windows: 2004/01–2004/12 and 2005/01–2005/12. Only the inversions in the second time window are for analysis and the first time window is designed to minimize the impacts of the

transition from GEOS-4 to GEOS-5 and from the LPJ-WSL scenario to other scenarios. In the above inversions, we included surface measurements from pan-Arctic sites but excluded satellite retrievals out of 50°S–50°N. The global inversions during 2005 also provided initial conditions and time-dependent boundary conditions for the nested grid simulations of the adjoint model. Following Turner et al. (2015), we did not optimize boundary conditions in the nested-grid inversions as did in Wecht et al. (2014). The nested grid inversions of the pan-Arctic were run at $1/2^\circ \times 2/3^\circ$ resolution from July 1, 2005 to Oct 1, 2005.

Specific humidity for bias correction was retrieved from the European Centre for Medium-Range Weather Forecasts (ECMWF)’s ERA-20C reanalysis product (<http://apps.ecmwf.int/datasets/data/era20c-daily>), averaged by the column between the surface and 3 km altitude (Houweling et al., 2014). The air mass factor and coordinates of satellite CH₄ retrievals have been included in the SCIAMACHY IMAV v6.0. For global-scale bias correction, we first optimized the GEOS-Chem 4-D CH₄ mixing ratios using only surface measurements and then sampled the modeled XCH₄ at the coordinates and time of SCIAMACHY retrievals and with local averaging kernels applied. Following Bergamaschi et al. (2009) and Houweling et al. (2014), only satellite retrievals between 50°S and 50°N were utilized. The XCH₄ differences between SCIAMACHY and GEOS-Chem are shown in Fig. S3a. A regression relationship was then built to represent the satellite system bias by proxy factors. Turner et al. (2015) suggested that it is more likely that grid squares residual standard deviation (RSD) in excess of 20 ppb are dominated by model bias in prior emissions. Thus, we excluded such grid squares in regressions. And satellite retrievals with low precisions (the ratio of retrieval precision error to retrieval is larger than 3%) were also removed from analysis. Following Houweling et al. (2014), we did not optimize bias correction functions in the inversion cycle in the concern that this process could

cause bias correction to incorrectly account for the uncertainties caused by unaccounted model errors or even the uncertain sources and sinks. As shown in Fig. S3d, bias correction reduced model-satellite differences greatly in tropical areas of America, Africa and South Asia and also reduced the differences in Australia and some areas of the United States. And the agreement between GEOS-Chem and SCIAMACHY is also improved at the global scale (Fig. S3c). However, the model-data agreement is deteriorated in East Asia. It could be caused by the overestimate of anthropogenic CH₄ emissions from China in the EDGAR dataset (Peng et al., 2016).

The results of the global inversions are presented in Table 2 and Fig. S4. There have been many studies that assimilated surface measurements and/or satellite retrievals into a CTM inverse model to constrain global CH₄ emissions, see Kirschke et al. (2013) for review. For instance, using the same observations suite, Bergamaschi et al. (2009) estimated that in 2004, CH₄ emissions in global, tropical (30°S–30°N), northern extratropical (30°N–90°N) and southern extratropical (90°S–30°S) zonal areas were 506.7 Tg CH₄ yr⁻¹, 323.5 Tg CH₄ yr⁻¹, 172.8 Tg CH₄ yr⁻¹ and 10.4 Tg CH₄ yr⁻¹, respectively. These large-scale estimates are consistent with our calculations: 284.5–319.6 Tg CH₄ yr⁻¹ (tropical), 165.3–206.6 Tg CH₄ yr⁻¹ (northern extratropical) and 10.0–13.9 Tg CH₄ yr⁻¹ (southern extratropical). This agreement could imply that the GEOS-Chem adjoint and TM5-4DVAR are consistent in the atmospheric transport, chemistry and inverse modeling methods. In contrast to Bergamaschi et al. (2009), our inversions allocate more emissions to extratropical regions. As a result, the tropical total (SATr + NAF + SAF + TrA) of the six inversions is in the range of 114.1–169.7 Tg CH₄ yr⁻¹, which is much lower than their estimate of 203.2 Tg CH₄ yr⁻¹. The likely reason for this discrepancy is that we did not optimize bias correction functions in the inversion cycle. Our posterior wetland CH₄ emissions estimated

in the Bern, CLM4Me, SDGVM and WSL scenarios are close to the estimate of 161 Tg CH₄ yr⁻¹ for 2003–2007 in Bloom et al. (2010). The latter was based on CH₄ and gravity spaceborne data to constrain large-scale methanogenesis. Our estimates are also close to the inferred wetland CH₄ emissions (175±33 Tg CH₄ yr⁻¹) by Kirschke et al. (2013). By using artificial neural networks, Zhu et al. (2013) estimated that from 1990 to 2009, annual wetland CH₄ emissions from northern high latitudes (> 45°N) were in the range of 44.0–53.7 Tg CH₄ yr⁻¹, agreeing with the estimates of the Bern, CLM4Me and SDGVM scenarios.

Fig. S4a shows that CH₄ fluxes are the highest in the Amazon, China, Southeast Asia, North America and Europe where there are either a large area of wetlands and rice paddies or advanced coal and oil industries or both. Our results indicate that the Eurasian temperate zone, including China, North America and Europe, emitted much more CH₄ than any other geographic zones (Table 2), implying the dominance of anthropogenic sources in the global CH₄ inventory. As presented in Fig. S4c, our inverse modeling reduced the CH₄ emissions from China, the Amazon basin and the Eurasian boreal region (scale factor < 1) but increased the emissions in Europe and Southeast Asia (scale factor > 1) relative to the prior.

Fig. S6 shows the difference between the modeled and observed CH₄ mixing ratios at NOAA ship board sampling stations and aircraft vertical profile sites under different wetland scenarios before and after the global scale inversions. For most scenarios, inversion improves the representation of CH₄ mixing ratios in GEOS-Chem at both marine and inland boundary layers and free troposphere. For example, the BERN scenario inversion reduced the bias by about 18 ppb for ship stations and about 6 ppb for aircraft sites. Also the DLEM scenario inversion reduced the bias by about 20 ppb for ship stations and about 19 ppb for aircraft sites. For the

CLM4Me and SDGVM scenarios with low prior biases, the inversions did not improve the performance. This could be caused by the errors introduced by the inversion process itself. For example, as the optimization is designed to address total emissions, the representation of diurnal variability in GEOS-Chem could be made worse during inversion.

Table S1. NOAA/ESRL stations used in the inversion.

Station ID	Latitude	Longitude	Altitude [m]	Station Name
ALT	82.45	-62.52	210.0	Alert, Nunavut, Canada
ZEP	78.90	11.88	475.0	Ny-Alesund, Svalbard (Spitsbergen), Norway and Sweden
SUM	72.58	-38.48	3238.0	Summit, Greenland
BRW	71.32	-156.60	11.0	Barrow, Alaska, USA
ICE	63.34	-20.29	127.0	Heimay, Vestmannaeyjar, Iceland
CBA	55.20	-162.72	25.0	Cold Bay, Alaska, USA
SHM	52.72	174.10	40.0	Shemya Island, Alaska, USA
UUM	44.45	111.10	914.0	Ulaan Uul, Mongolia
NWR	40.05	-105.58	3526.0	Niwot Ridge, Colorado, USA
AZR	38.77	-27.38	40.0	Terceira Island, Azores, Portugal
WLG	36.29	100.90	3810.0	Mt. Waliguan, People's Republic of China
BMW	32.27	-64.88	30.0	Tudor Hill, Bermuda, UK
IZO	28.30	-16.48	2360.0	Tenerife, Canary Islands, Spain
MID	28.21	-177.38	7.7	Sand Island, Midway, USA
ASK	23.18	5.42	2728.0	Assekrem, Algeria
MLO	19.53	-155.58	3397.0	Mauna Loa, Hawai, USA
KUM	19.52	-154.82	3.0	Cape Kumukahi, Hawaii, USA
GMI	13.43	144.78	6.0	Mariana Islands, Guam

RPB	13.17	-59.43	45.0	Ragged Point, Barbados
CHR	1.70	-157.17	3.0	Christmas Island, Republic of Kiribati
SEY	-4.67	55.17	7.0	Mahe Island, Seychelles
ASC	-7.92	-14.42	54.0	Ascension Island, UK
SMO	-14.24	-170.57	42.0	Tutuila, American Samoa, USA
CGO	-40.68	144.68	94.0	Cape Grim, Tasmania, Australia
CRZ	-46.45	51.85	120.0	Crozet Island, France
TDF	-54.87	-68.48	20.0	Tierra Del Fuego, La Redonda Isla, Argentina
PSA	-64.92	-64.00	10.0	Palmer Station, Antarctica, USA
SYO	-69.00	39.58	14.0	Syowa Station, Antarctica, Japan
HBA	-75.58	-26.50	33.0	Halley Station, Antarctica, UK
SPO	-89.98	-24.80	2810.0	South Pole, Antarctica, USA

Table S2. NOAA aircraft profiles used for validation.

CODE	Location	Latitude (deg)	Longitude (deg)	Start Date	End Date
PFA	Poker Flat, Alaska, United States	65.07	-147.29	06/27/1999	06/05/2015
ESP	Estevan Point, British Columbia, Canada	49.6	-126.4	11/22/2002	06/09/2015
DND	Dahlen, North Dakota, USA	48.1	-98.0	09/21/2004	05/31/2015
LEF	Park Falls, Wisconsin, USA	45.9	-90.3	04/10/1998	05/28/2015
FWI	Fairchild, Wisconsin, USA	44.7	-91.0	09/20/2004	11/18/2005
NHA	Worcester, Massachusetts, USA	43.0	-70.6	09/21/2003	06/10/2015
BGI	Bradgate, Iowa, USA	42.8	-94.4	09/13/2004	11/18/2005
HFM	Harvard Forest, Massachusetts, USA	42.5	-72.2	11/11/1999	11/18/2007
WBI	West Branch, Iowa, USA	42.4	-91.8	09/14/2004	05/28/2015
OIL	Oglesby, Illinois, USA	41.3	-88.9	09/16/2004	11/19/2005
THD	Trinidad Head, California, USA	41.0	-124.2	09/02/2003	05/16/2015
BNE	Beaver Crossing, Nebraska, USA	40.8	-97.2	09/15/2004	05/11/2011
CAR	Briggsdale, Colorado, USA	40.6	-104.6	11/09/1992	04/21/2015
HIL	Homer, Illinois, USA	40.1	-87.9	09/16/2004	05/21/2015
TGC	Sinton, Texas, USA	27.7	-96.9	09/09/2003	06/05/2015
HAA	Molokai Island, Hawaii, USA	21.2	-158.9	05/31/1999	04/22/2008
RTA	Rarotonga, Cook Islands	-21.3	-159.8	04/16/2000	05/29/2015

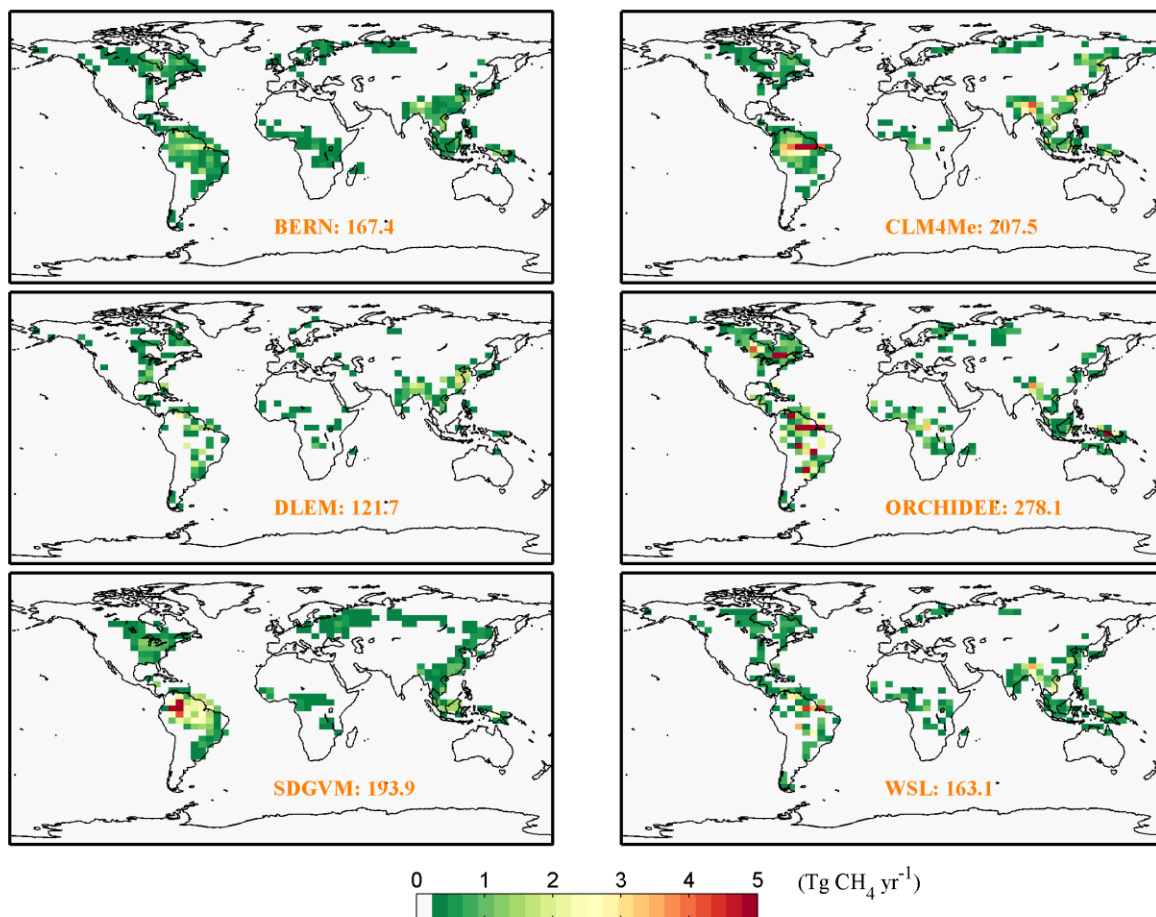


Figure S1. Average of prior wetland CH_4 annual emissions during 2004–2005 from six different wetland biogeochemical models used for the GEOS-Chem global inversion at $4^\circ \times 5^\circ$ resolution. Annual total emission (orange) is presented in units of $\text{Tg CH}_4 \text{ yr}^{-1}$.

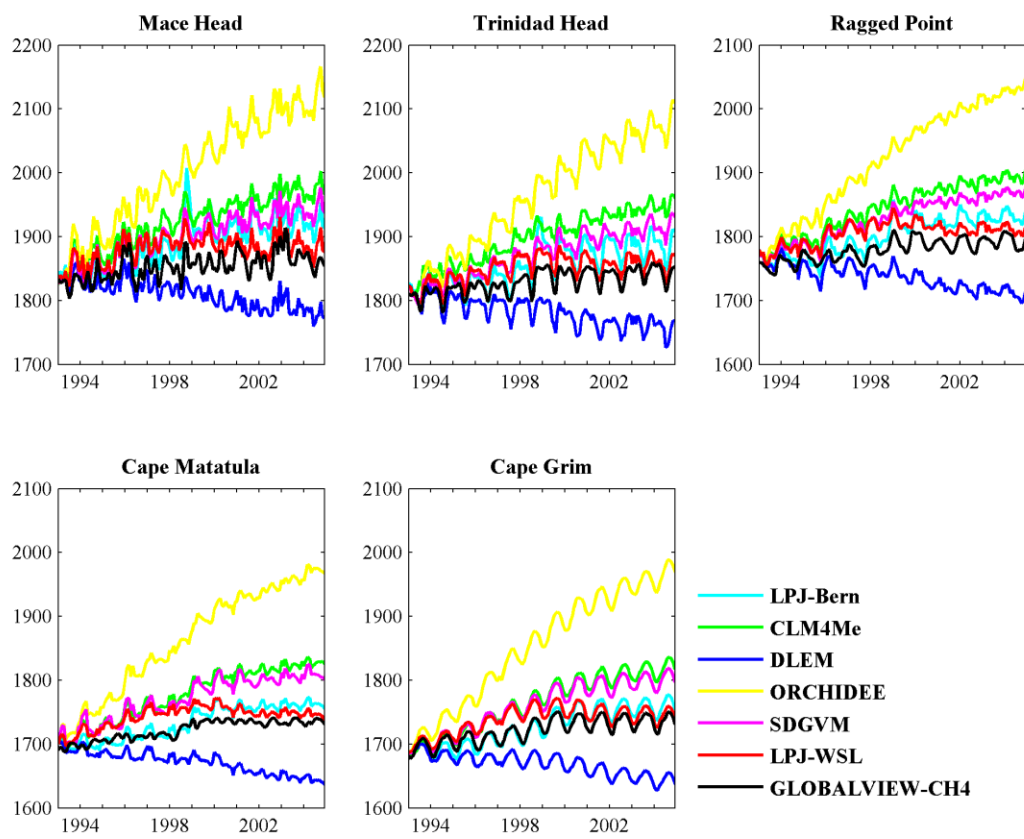


Figure S2. The comparison between the GEOS-Chem simulated and GLOBALVIEW-CH₄ atmospheric CH₄ (units: ppbv) at five stations (Mace Head, Ireland; Trinidad, California; Ragged Point, Barbados; Cape Matatula, Samoa; Cape Grim, Tasmania). The wetland CH₄ emissions used are pre-optimized model simulations provided by the WETCHIMP project.

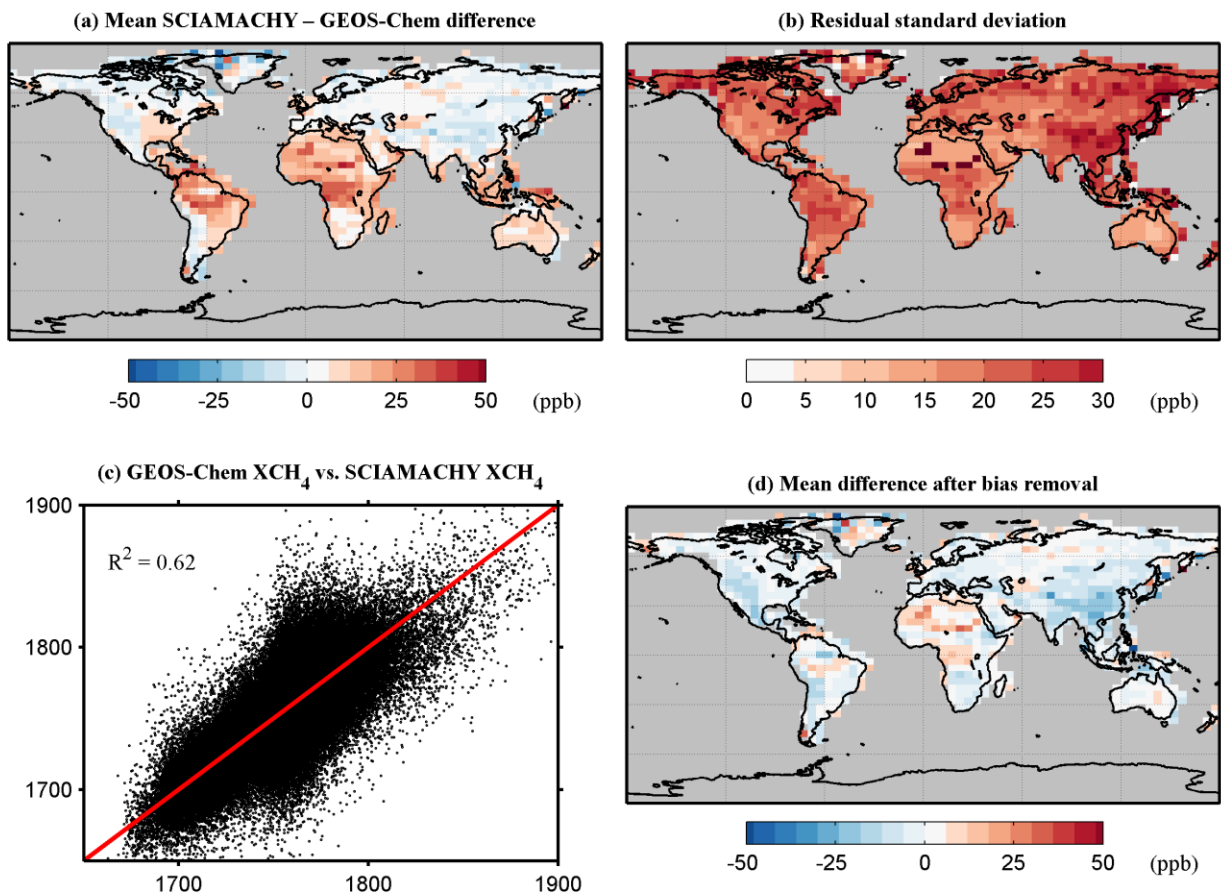


Figure S3. Comparison of column averaged CH₄ mole fractions from SCIAMACHY with those from GEOS-Chem model calculated with prior emissions. (a and b) show the mean bias and residual standard deviation of the satellite-model difference, (c) shows the comparison of the model (x axis) and satellite (y axis) XCH₄ after applying the “latitude + humidity” correction from the linear regression (weighted R² is shown inset and the red 1:1 line is also shown), and (d) shows the satellite-model difference after bias removal.

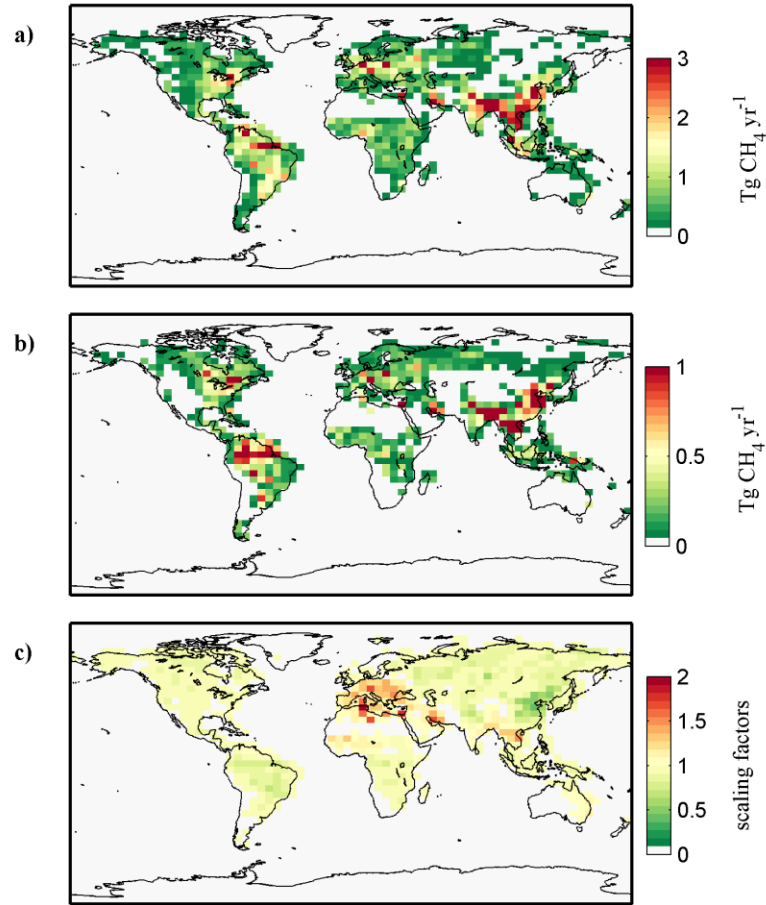


Figure S4. Optimized global CH₄ emissions and emission scale factors in 2005 at 4° × 5° resolution. Emission scale factor is defined as posterior emissions relative to prior emissions. a) Posterior CH₄ emissions averaged over inversions of six scenarios; b) standard deviation of posterior CH₄ emissions over inversions of six scenarios; c) optimized emission scale factors averaged over inversions of six scenarios.

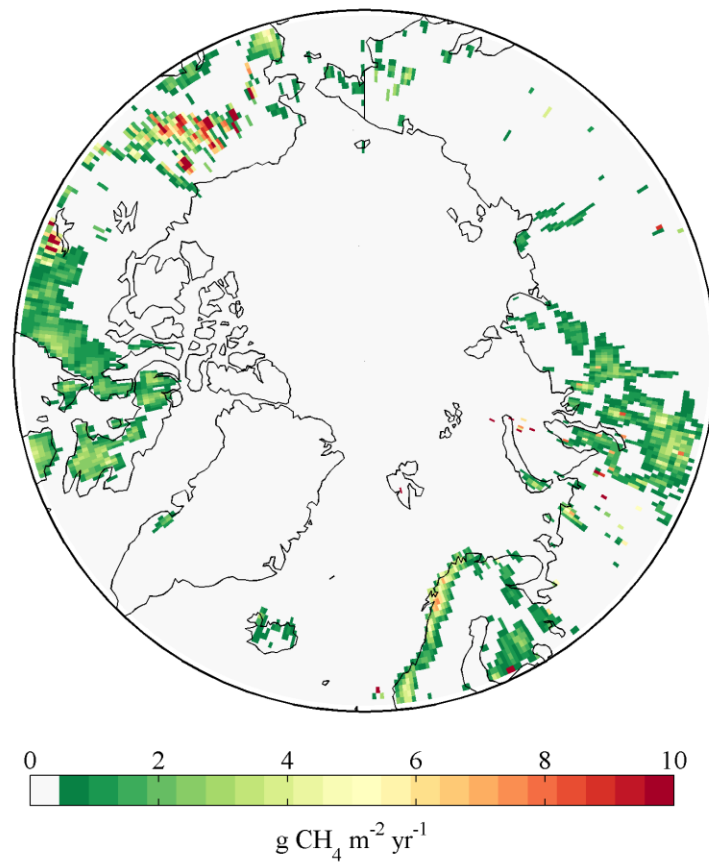


Figure S5. Posterior CH₄ emissions from the pan-Arctic in 2005 estimated by the inversion of the “DLEM wetland only” scenario. The “DLEM wetland only” scenario uses the simulated wetland CH₄ emissions from the DLEM model and does not incorporate CH₄ emissions from pan-Arctic lakes.

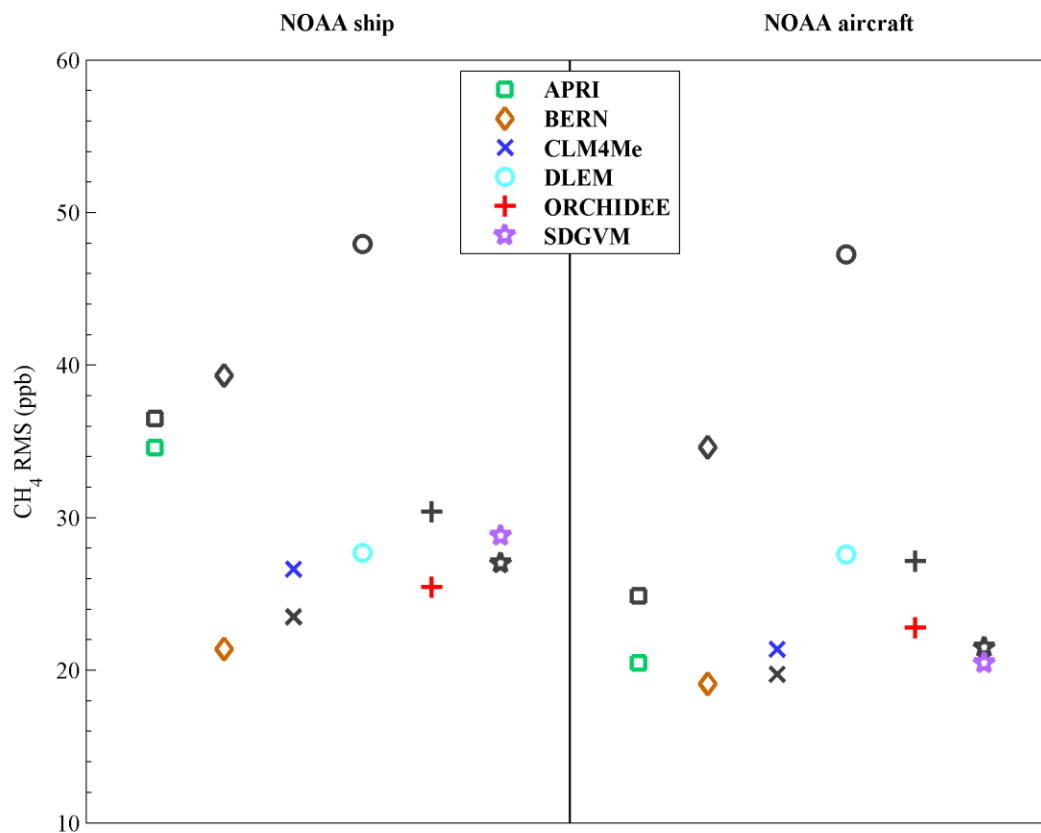


Figure S6. Evaluation of posterior GEOS-Chem CH₄ mole fractions from the global inversions with independent data sets. The plot shows the root mean square (rms) of differences between the modeled and the observed CH₄ mixing ratios. Black symbols indicate the rms of the forward GEOS-Chem runs.